STUDY OF THE FEASIBILITY OF DETERMINING BUBBLE CONCENTRATION ACROSS LAKE ONTARIO USING UNDERWATER ACOUSTIC TRANSMISSION LOSS

Part 1. Mathematical modelling of sound propagation in Lake Ontario

Contractor   Professor Sergey N. Gurbatov
Chair of Acoustics
Department of Radiophysics
University of Nizhny Novgorod, Russia

University of Nizhny Novgorod

March, 1993

TABLE OF CONTENTS

The scientific report is prepared under the contract with Atmospheric Enviroment Service at the Acoustics Chair of the University of Nizhny Novgorod, Russia.

List of participants

Sergey N.Gurbatov — Head of Acoustics Chair, Professor

Nickolay V.Pronchatov-Rubtsov — Associate Professor
Oleg V.Lebedev — Assistant Professor
Ivan V.Pavlov — Junior researcher
Alexander M.Sutin — Professor

Translated by Ivan V.Pavlov and Nick S.Gurbatov (student).

University of Nizhny Novgorod
Department of Radiophysics
23 Gagarin Avenue
Nizhny Novgorod, 603600, Russia
phone (8 312) 65 61 14
telex 224846 UNIGO SU

SUMMARY

The report is the first part of the work devoted to the investigation of the feasibility of the distant acoustic determination of bubble concentrations in the subsurface layer of Lake Ontario.

In this part the physical mechanisms on base of which the distant sounding of the air bubbles in water is possible are shortly discussed. Here the principles of the determination of bubble concentration in the subsurface layer measuring the attenuation of the acoustical signal are presented, the hydrological parametrs of the path of propagation between the western tip of Toronto Island and the mouth of Welland Canal are given. The acoustic properties of the bottom are discussed as well.

The comparison of different methods for the mathematical modelling of sound propagation in the inhomogeneous range-dependent waveguide are presented and the calculations of acoustic fields along the above-mentioned path are carried out for the depths from 10 m to 40 m within the frequency band from 100 Hz to 10 kHz . It is shown that in winter season, when the sound speed is close to constant, the average intensity in the end of the path slightly depends both on the receiver depth and on the source frequency. At the same time, in summer, when the upper layer of Lake is heated, the subsurface waveguide exists. Because of it the field is localized near the bottom and the signal level decreases both with the increase of source frequency and with the decrease of reciever depth. It is shown that the signal level depends rather strongly (especially in summer season) on the acoustic properties of the bottom.

Chapter 1.
INTRODUCTION

1.1 INFLUENCE OF AIR BUBBLES ON PROPAGATION, ABSORPTION AND SCATTERING OF SOUND.

Air bubbles in water significantly affect the sound propagation. It can be explained that in a wide frequency band the scattering and absorption are of resonant nature. Thus, at the resonant frequency scattering cross section of an air bubble could be more than 1000 times larger than its geometrical cross section. If the bubble concentration is rather high water compressibility changes considerably and sound velocity changes respectively. Moreover, among the all possible sound scatterers bubbles have the most clearly expressed nonlinear properties. All these facts allows to consider acoustic methods as the most adequate ones for the distant diagnostics of air bubbles.

A bubble as a resonance system can be described by its quality factor Q and natural (resonance) frequency f_o, which in adiabatic approximation [1,2] is given by expression

$$f_o = \frac{1}{2 \pi a} \left[\frac{3\gamma \, p_o}{\rho} \right]^{1/2} , \qquad (1.1)$$

where a is a bubble radius, $\gamma = c_p / c_v$ – index of adiabat (in the air $\gamma = 1.4$), p_o – pressure in a bubble in the absence of sound wave, ρ – water density. The resonant frequency f_o of the air bubble located at the depth z can be estimated as

$$f_o = 327/a \, (\, 1 + 0.1z \,)^{1/2} , \qquad (1.2)$$

where f_o is in Hz , depth z – in metres , bubble radius a – in

centimetres.

When a plane acoustic wave of the frequency f is falling on an air bubble, its volume changes harmonically so it radiates the spherical sound wave. Moreover, a part of acoustic energy is absorbed due to the viscosity and heat conductivity . The efficiency of absorption and scattering is described by the absorption cross section σ_a and scattering cross section σ_s defined as

$$\sigma_s = W_s / I_t \; ; \; \sigma_a = W_a / I_t \; , \qquad (1.3)$$

where I_t is the intensity of an incident wave, W_s - acoustic power scattered in all directions, W_a - acoustic power absorbed by an air bubble. For the scattering cross section σ_s and absorption cross section σ_a of a single bubble one can write

$$\sigma_s = \frac{4 \pi a^2}{[(f_o / f)^2 - 1]^2 + Q^{-2}} \; , \qquad (1.4)$$

$$\sigma_a = \frac{4 \pi a^2 (Q^{-1}/ka - 1)}{[(f_o / f)^2 - 1]^2 + Q^{-2}} \; , \qquad (1.5)$$

where $k = 2\pi f/c_o$, c_o is sound speed in the liquid free of bubbles. It can be easily seen from (1.4), (1.5) that the scattering and absorption increase if the frequency of an acoustic waves coincides with the resonant frequency of a bubble.

When wave propagates in the bubbly medium, both coherent and incoherent components appear in the scattered field. The intensity of the incoherent component is proportional to the number of bubbles in the scattering volume. If bubbles are of different sizes, their size distribution can be described by function $n(a)$. Then $n(a) \, da$ is the number of bubbles with sizes from a to $a + da$ in an unit volume (m^3).

Scattering on the bubbles of different sizes might be characterized by the volume scattering coefficient m_v

$$m_v = 4\pi \int_0^\infty \frac{n(a)\, a^2\, da}{[(\omega_o/\omega)^2 - 1]^2 + Q^{-2}} \; ; \; \omega = 2\pi f, \; \omega_o = 2\pi f_o, \quad (1.6)$$

which is equal to the ratio of the acoustic power scattered by a unit volume in a unit angle to the intensity of the incident wave. Since the scattering is of resonance nature, the measurements made at different frequencies give us the possibility to determine the size distribution.

For the coherent component of an acoustic field the water with air bubbles often can be treated as a continuous medium with the effective sound speed c_{eff} and with the greater absorption, which is described by the absorption coefficient in a bubble media $\alpha(\omega)$. As a rule, the density of the water with suspended air is only slightly different from the density of the water free of bubbles. So the dispersion equation $K = K(\omega)$ for a monochromatic wave might be written as [3]

$$K^2 = \frac{\omega^2}{c_o^2} + \int_0^\infty \frac{4\pi\, n(a)\, a\, da}{(\omega_o/\omega)^2 - 1 + i/Q} \; ; \; K = \omega/c_{eff}. \quad (1.7)$$

For a relatively small bubble concentration, when the sound absorption on the wavelength is small, (1.7) may be reduced to

$$K = \frac{\omega}{c_o - \Delta c} + i\alpha , \quad (1.8)$$

where Δc is the addition to the sound speed which appears due to a presence of bubbles. When α/K, $\Delta c/c_o \ll 1$, the following expression is valid

$$\Delta c = 2\pi c_o \int_0^\infty \frac{n(a)[\,(\omega_o/\omega)^2 - 1\,]a\, da}{K_o[\,((\omega_o/\omega)^2 - 1)^2 + Q^{-2}\,]} , \quad (1.9)$$

$$\alpha = 2\pi \int_0^\infty \frac{n(a)\, a\, da}{K_o[\,((\omega_o/\omega)^2 - 1)^2 + Q^{-2}\,]} . \quad (1.10)$$

4

Analysis of these expressions shows that if we may neglect the variability of the distribution function $n(a)$ at the width of the resonant curve, then $\Delta c \approx 0$. So in this case the absorption is determined only by the concentration of resonant bubbles of the correspondent frequency and does not depend on their quality factor. The numerical expression for the absorption coefficient a (1/m) is

$$a = a(\omega) \approx 725 \ n(a_r) \ a_r^3 \ , \qquad (\ 1.11 \ )$$

where a_r is the radius of resonant bubbles (cm) (their resonant frequency is $\omega = 2\pi f$ - see (1.1)).

Thus, since the bubbles have such strongly pronounced resonant and nonlinear properties, methods based on the following effects might be used for the measurements of the bubble concentration:

- measurement of the sound attenuation,
- measurement of volume scattering coefficient,
- measurement of volume nonlinear scattering coefficient.

The detailed investigation of this problem can be found in [4 - 20]. It must be noticed that some methods of acoustic diagnostics was developed and experimentally approved in IAP and in the University of Nizhny Novgorod [21 - 25].

Our purpose is to investigate the possibility of the distant determination of bubble concentration in the subsurface water layer of Lake Ontario. That is why we pay some attention to the review of [3,26]. The results presented in these papers let us hope that this problem can be solved in general.

In [26] the bubble induced attenuation of acoustic signal of frequencies 1 kHz, 3kHz and 8kHz has been measured at the fixed acoustic shallow water range (path lenght 10.5 km, depth - $H = 30 \pm 2$ m). The experiments showed, that the attenuation due to suspended air increase by the m'th power of wind speed U (m between 3.5 and 4.5). The increase of transmission loss was explained by the growth of bubble concentration in the subsurface layer due to increase of the

wind speed. Hence, the signal attenuation can carry the useful information about the bubble concentration in the subsurface layer.

In the same time, in paper [3], basing on the results of [18,27], it was shown that the concentration of bubbles $n(a)$ which appears due to the sea surface agitation may be parameterized and written as

$$n(a) = M_o \; G(a,z) \; \mathcal{X}(U) \; \mathcal{Y}(z,U), \qquad (\; 1.12 \;)$$

where U is the wind speed in m/s (its basic value was $U = 13$ m/s), z – depth (m),

$$\mathcal{Y} \; (z,U) = exp \; [\; -z/L(U)], \qquad (\; 1.13 \;)$$

$$L(U) = \begin{cases} 0.4 \quad , \; U \quad 7.5 \; \text{m/s} \\ 0.4 + 0.115(\; U - 7.5 \;), \; U > 7.5 \; \text{m/s}, \end{cases}$$

$$N_o = 1.6 \; x \; 10^{10} \; m^{-4}, \qquad \mathcal{X}(\; U \;) = (\; U/13 \;)^3,$$

$$G(a,z) = \begin{cases} (\; a/a_1)^2 \quad , \quad a < a_1 \\ 1 \qquad\qquad , \quad a_1 \leqslant a \leqslant a_2 \qquad (\; 1.14 \;) \\ (\; a_2/a \;)^{d(z)}, \quad a > a_2 \end{cases}$$

and the limit bubble sizes a_1 and a_2 are expressed as

$$a_1 = (\; 34 + 1.24 \; z \;) \; x \; 10^{-6}(\; m \;),$$

$$a_2 = 1.6 \; a_1 \; , \qquad\qquad\qquad (\; 1.15 \;)$$

$$d(z) = 4.37 + (\; z \; / \; 2.55 \;)^2.$$

Thus, using (1.12) and measuring the transmission loss at different frequencies it might be possible in some cases to solve the inverse problem – to reconstruct the size distribution. Then, one of the questions appearing is the feasibility of parameterization for the size distribution $n(a)$ of subsurface bubbles in inner lakes and Lake Ontario as well.

6

1.2 PHYSICAL FOUNDATION OF DETERMINING THE BUBBLE CONCENTRATION IN SUBSURFACE BUBBLE LAYERS.

As it follows from the results obtained in previous chapter, the attenuation of a signal of rather high frequency f mainly depends on the concentration of resonant bubbles (see 1.1). If a plane wave propagates in the medium with homogeneously distributed bubbles, its amplitude decreases as

$$p = p_0 \, exp(-\alpha \, r)$$

Thus, measuring the transmission loss (TL) on the path of range r

$$TL = 20 \, lg \frac{p_0}{p} = 10 \, lg \frac{I_0}{I} = \alpha \, r \, 20 \, lg \, e = 8.64 \, \alpha \, r \quad (\, 1.16 \,)$$

we can find out the attenuation coefficient $\alpha = TL \, / \, 8,64 \, r$, and then – the concentration of resonant bubbles (see 1.11).

However, the problem becomes more complicated in natural waveguides. It is concerned with the finity of a bubble layer. Here the sound field has a very complex structure so the simple dependence of TL on attenuation coefficient α fails. Because of it the diagnostics of subsurface bubble layer requires the more detailed analysis.

In this chapter we will try to show clearly the physical base of sound field attenuation in a waveguide with subsurface bubble layer and will discuss both the principal feasibility of determining the bubbles concentration and the difficulties which appear when solving the problem.

To calculate the acoustic fields of high frequency one can use the ray approach [28]. For the case of layered waveguide, when the sound speed c depends only on depth z ($c = c(z)$), the trajectories of rays might be calculated from Snell's law:

$$cos \, \chi(z) \, / \, c(z) = const,$$

where $\chi(z)$ – the grazing angle at any horizon z. In the framework of ray approximation the energy flows within the ray tube. It allows to find out the field amplitude using the

conservation law for power flux dW through the cross section area of the tube dS :

$$dW = I \, dS = const, \qquad I = p^2,$$

where I is the intensity of sound field.

Let the source to be positioned at the depth z_1 and the receiver – at the point with coordinates r and z (Fig.1.1).
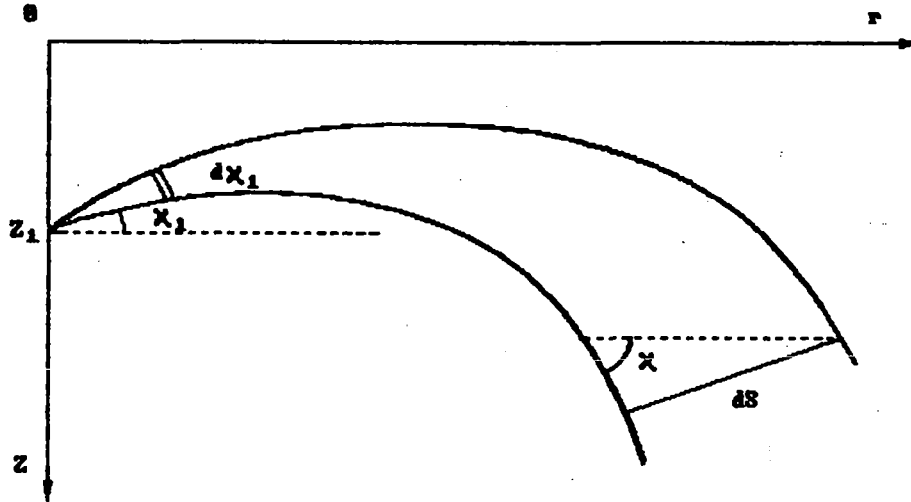

Fig.1.1

Considering the ray bundle $d\chi_1$ (the tube width), which leaves the source at the angle χ_1, and taking into account the z-symmetry it is easy to obtain for the point with coordinates r,z:

$$dS = 2\pi r \left| \frac{dr}{d\chi_1} \right| \sin \chi \, d\chi ,$$

$$dW = (W/2) \cos \chi_1 \, d\chi_1$$

and, therefore

$$I = \frac{W \cos \chi_1}{4\pi r \left| \dfrac{dr}{d\chi_1} \right| \sin \chi} E(\chi_1) . \qquad (1.17)$$

Here $E = E(\chi_1)$ - an attenuation factor introduced to account for dissipation and reflection losses. In a general case, there are some rays which might come into the point of receiver. Because of it one has to sum their amplitudes and phases to calculate the field. Due to that at the long distances the field structure becomes very complex and unsteady (small changes of sound speed profile could strongly influence on the rays phases). Thus, it is more expediently to use the averaged description.

For the plane layered waveguide the ray trajectory $z = z (r)$ has a range periodicity called ray cycle. The cycle length $D(\chi_1)$ (see Fig.1.2) depends also on the source depth.
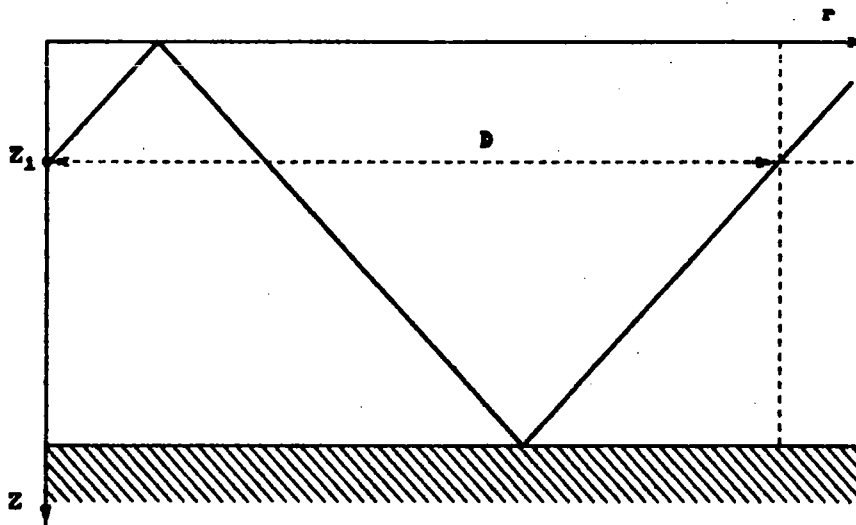

Fig.1.2

At long distances, where $r \gg D$ to obtain the averaged on the cycle length intensity of the field the contribution of a ray bundle $d\chi_1$ (I in 1.17) is to be weighted by the probability that it irradiates a receiver at depth z in the course of complete cycle near range r. This probability might be written as $(2 \mid \partial r/\partial \chi_1 \mid d\chi_1)/ D(\chi_1)$. Factor 2 appears because a ray cuts the z horizon twice per cycle. If we consider the power of source $W = 4\pi$, then $\mid p \mid^2 = I = 1/r^2$. Using (1.17) and taking into account the angle symmetry we can write the expression for averaged intensity [29]:

$$\bar{I} = (4/r)\int\limits_{0}^{\pi/2} \frac{E(\chi_1 ,r) \cos \chi_1}{D(\chi_1) \sin \chi(\chi_1)}\, d\chi_1 , \qquad (1.18)$$

where $\chi = \chi(\chi_1)$ is the inclination (grazing angle) of ray at the receiver horizon.

Within one cycle a ray once touches the bottom, being attenuated in $| V(\chi_h) |^2$ times in it. Here χ_h - is the ray inclination at the bottom and $V(\chi_h)$ is the reflection coefficient of the bottom.

If we consider attenuation coefficient $\alpha(z)$ to be depending on depth, then the factor concerned with dissipation within one cycle is

$$E_v = exp (- 2 \int\limits_{0}^{l_o} \alpha(z) l\, dl) , \qquad (1.19)$$

where l_o is the lenght of ray trajectory.

For the path of length r the number of cycles $N = r/D(\chi_1)$ and, thus, the attenuation factor in 1.18 might be written as

$$E(\chi_1) = \left| V^2 E_v \right|^{r/D(\chi_1)}. \qquad (1.20)$$

Expressions (1.18) - (1.20) allows to obtain the range dependence of averaged sound transmission loss in a range - independent waveguide. The generalization for a range-dependent ducts is given in [30] and is used in this work for calculation of sound field intensity in Lake Ontario.

Let's consider some particular cases of sound propagation in the isovelosity waveguide. In a homogeneous water layer with $c = c_1 = c_h = const$ (such profile of sound speed is close to the winter conditions of propagation in Lake Ontario) the cycle length is:

$$D = 2 H / tg \chi_1 , \qquad (1.21)$$

where H is a thickness of water layer - the depth of a waveguide (see Fig.1.2). If $\alpha = 0$ and $| V | = 1$, then from

(1.18) we have

$$\bar{I} = \frac{4}{r} \frac{1}{2H} \int_0^{\pi/2} d\chi_1 = \frac{\pi}{r\,H} . \qquad (1.22)$$

This formula shows the well known cylindrical law of field decrease. Returning to a general case we can rewrite the expression for average intensity in the following form :

$$\bar{I} = \frac{2}{rH} \int_0^{\pi/2} A(\chi_1)\, d\chi_1 , \qquad (1.23)$$

$$A(\chi_1) = \frac{2\,H\,E(\chi_1, r)\,\cos\chi_1}{D(\chi_1)\,\sin\chi(\chi_1)} . \qquad (1.24)$$

Here factor A is a factor which accounts both the effects of attenuation and the effects, concerned with variability of sound speed, i.e. with stratification. It might be seen, that for the isovelosity homogeneous waveguide with $\alpha = 0$ and $|V| = 1$ factor $A = 1$.

If we suppose isovelosity water layer to be settled down on a liquid bottom without absorption ($c_b > c_1$), then one can introduce the critical angle χ_*, which might be calculated from Snell's law:

$$\cos\chi_* = \frac{c_1}{c_b} ; \qquad \chi_* = \left[\frac{2\Delta c}{c_b}\right]^{1/2} \qquad (1.25)$$

Here c_b – is the sound speed in the bottom and $\Delta c = c_b - c_1$. If the angle of ray inclination at the bottom $\chi_h = \chi_1 < \chi_*$, then $V = 1$, otherwise V becomes less. Taking into account the fact that for $r/D \gg 1$ the number of ray reflections is great, obviously, the rays which leave the source at the angles $\chi_1 > \chi_*$ are being attenuated almost completely (see 1.20). It allows to change the upper limit of integration in (1.23) from $\pi/2$ to χ_*.

Now let's consider the homogeneous bubble layer of

thickness h and constant absorption coefficient a near the surface of considered waveguide. From Fig.1.3 it is seen that within one cycle attenuation factor is

$$E_v = exp\ (\ -\ 2aS_*\ )\ =\ exp\ (\ -\ 4\ a\ h\ /\ sin\ \chi_1\ ),\quad (\ 1.26\ )$$
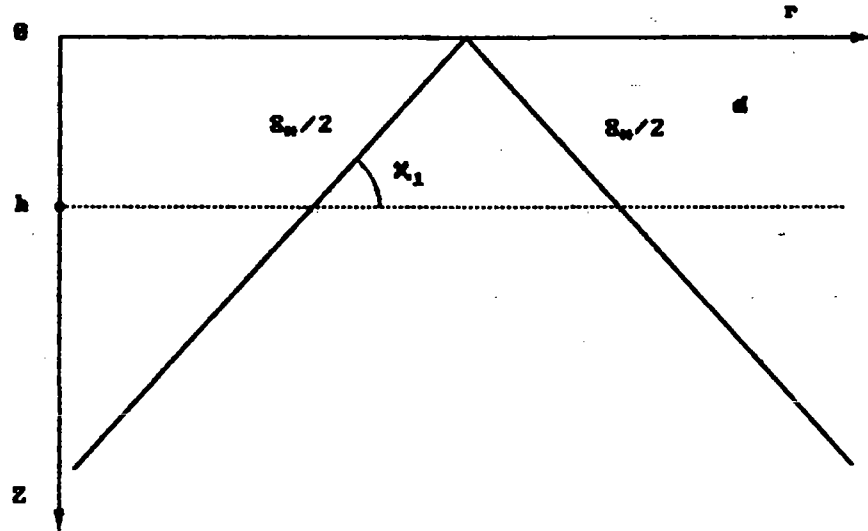

Fig.1.3

where $S_* = 2\ a\ h\ /\ sin\ \chi_1$ - the length of the ray cycle part within the bubble layer. Then Eq.1.24 might be rewritten as follows (for the isovelosity waveguide):

$$A = exp\ \left[-\ \frac{2a\ h\ r}{H\ cos\ \chi_1} \right]\ \approx exp\ \left[-\ \frac{2a\ h\ r}{H}\ -\ \frac{a\ h\ r\ \chi_1^2}{H} \right].\quad (\ 1.27\ )$$

Here we took into account that the main contribution is being made by the rays of angles $\chi_1 < \chi_*$.

From (1.27) we can make the important conclusion, that at small angles of inclination A does not depend on χ_1. The reason is that for the rays with $\chi_1 \ll 1$ S_* is rahter great, butthe number of cycles is small. And these effects compensate each other.

There are two main effect concerned the attenuation in a thin bubble layer. The first is the decrease of amplitudes

of all the rays : they decreases as $exp(-2\alpha hr/H)$. And the second one is the narrowing of angle spectrum up to $\chi_{bbl} = (H/\alpha hr)^{1/2}$. If $\chi_{bbl} \gg \chi_*$ we can neglect this effect, and then from (1.22),(1.27) one can obtain the following expressions for averaged intensity and transmission loss:

$$\bar{I} = \frac{2}{rH} \chi_* \, exp(-2\alpha hr/H) \qquad (\ 1.28\ )$$

$$TL = 10 \, ln \, I/I_o = TL_o + 8.64 \, \alpha rh \, / \, H = TL_o + \Delta TL \quad (\ 1.29\ )$$

Here $TL_o = 10ln(rH/2\chi_*)$ transmission loss in the waveguide free of bubbles and the second item describes the additional losses due to the bubble layer. From the comparison of this expression with TL for the homogeneous bubbly media (1.16) it is seen that for such a layer TL is less in h/H times. The reason is that only the part of a ray trajectory goes through a bubble layer. It must be mentioned, that the the additional loss ΔTL is proportional to the quantity of bubbles along all the path ($\Delta TL \sim \alpha rh \sim n\,S$, where $S = rh$).

It might be shown that the small absorption in bottom does not make the situation considerably worse for isovelosity guide. The difficulties arise in a case of stratified waveguide, especially for "summer" kind of stratification, when sound speed at the bottom is less than at the surface. In such a waveguide some do not reach the bubble layer, so it makes the transmission loss to be a complex function of absorption.

In an arbitrary case to calculate averaged intensity (1.18) analytically seems to be impossible, so we have to do it numerically. Some results are presented below. The calculation has been made for the following model of waveguide :.
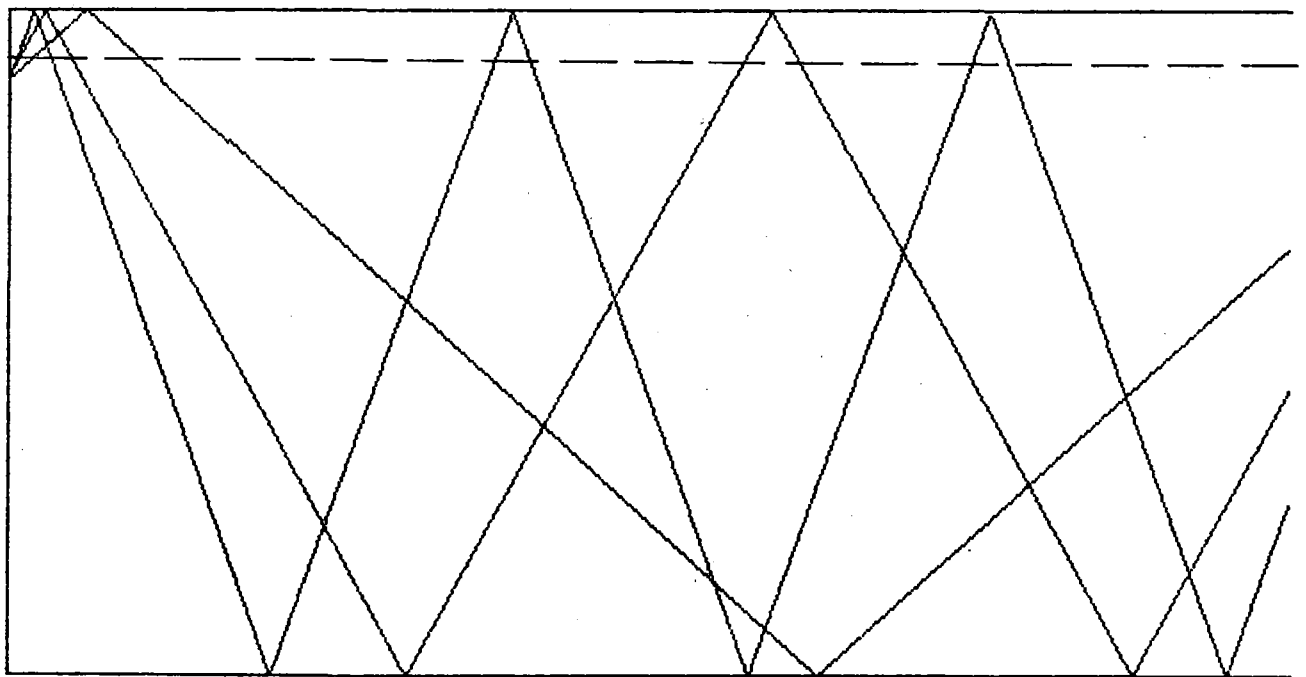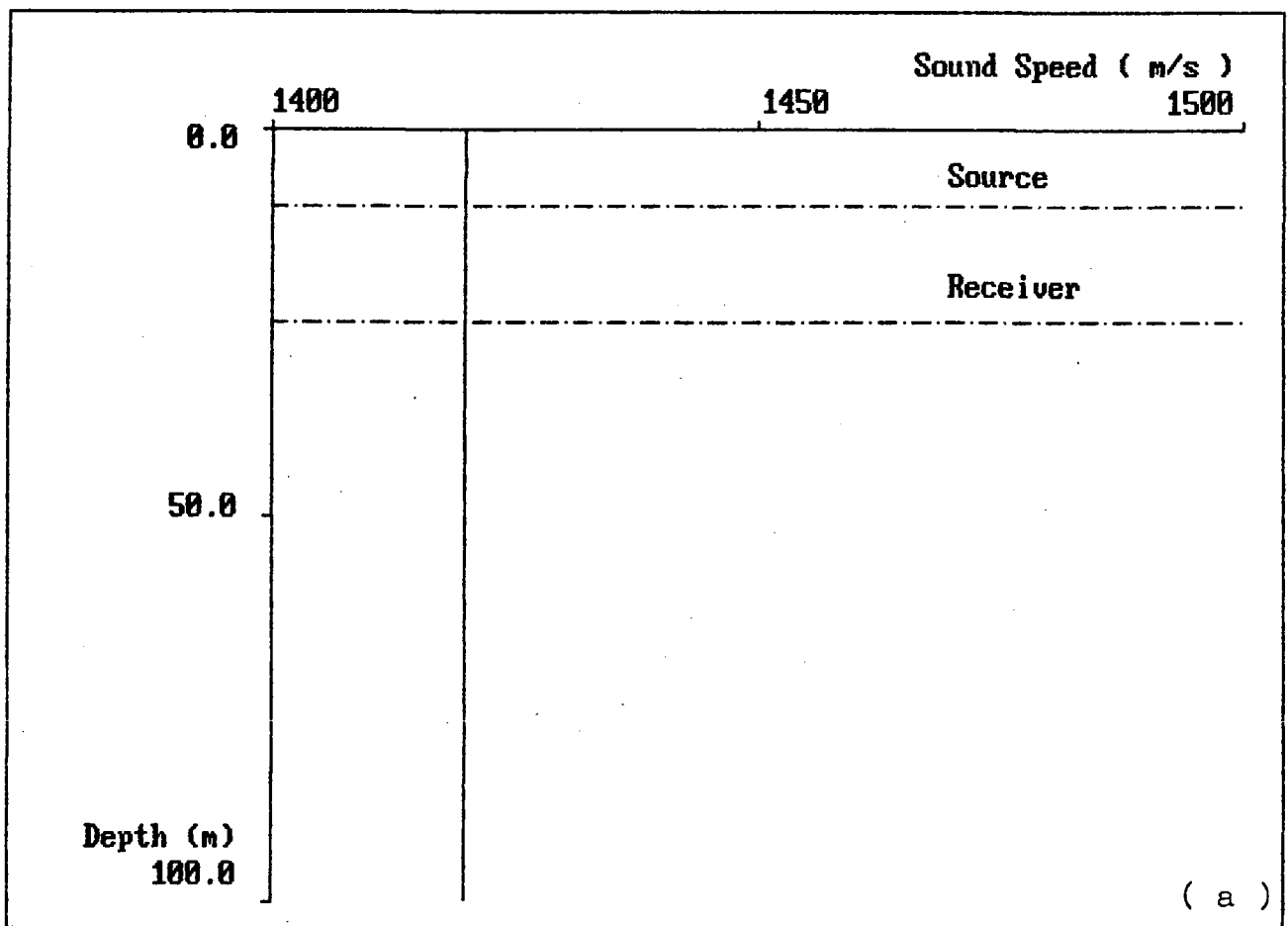
The path length is 20 km, sound speed in bottom $c_b = 1580$ m/s, sound spped in water at the bottom $c_h = 1420$ m/s(critical angle $\chi_* \approx 0.47$ rad ≈ 28 deg, depth of the waveguide $H = 100$ m.

Two models of bottom has been used : half-space without and

with losses (the imaginary part of the refraction index $\eta=0.008$). Model of the bubble layer : thickness h = 6 m, absorption coefficient α = 0.0025. (For the case of the waveguide with homogeneously distributed bubbles, i.e. $h = H$, the bubble induced loss would be ATL = 432 dB − see 1.29). Typical ray trajectories are depicted for the path of 2 km length.

At Fig.1.4(a) the isovelosity waveguide − "winter" profile is shown. For this profile of sound speed the ray trajectories are presented in Fig.1.4(b). At Fig.1.5 angle distribution of factor A is shown for bottom without (a) and with (b) absorption. As it might be seen from these figures, for this case the effect is clear : all the rays radiated reach the subsurface bubble layer and are attenuated in it, so it leads to the decrease of signal level. At Fig.1.6 (a),(b) the range dependence of integral averaged intensity of field is depicted for both models of bottom respectively. (Here and below, solid line − with bubble layer, dashed line − out of bubble layer). It is remarkable, that in an isovelosity waveguide the introducing of the bottom absorption leads to general decrease of signal level approximately on 5 dB, but almost does not affect the bubble layer induced attenuation value (at the Fig.1.6 $ATL \approx 26dB$). This result is in a good agreement with (1.29). Calculating ATL from (1.29) one can find that the bubble induced attenuation in the case of layer thickness 6 m is less than for homogeneously distributed bubbles in h/H = 0.06 times.

In a case of "summer" profile of sound speed the picture seems to be more complicated (Fig.1.7(a)). As it is seen from Fig.1.7(b) there are three groups of rays (A factor for these rays presented on Fig.1.8(a),(b) for both models of bottom): A − the rays of small grazing angles, which do not reach the bubble layer; B − the rays, which reach the layer but don't touch the surface − their inclination at the bound of bubble layer is small and because of it the attenuation of these rays is great; C − the rays reflected by the surface. The averaged field range distribution for this stratification is presented at Fig.1.9(a),(b). It is seen, that here the
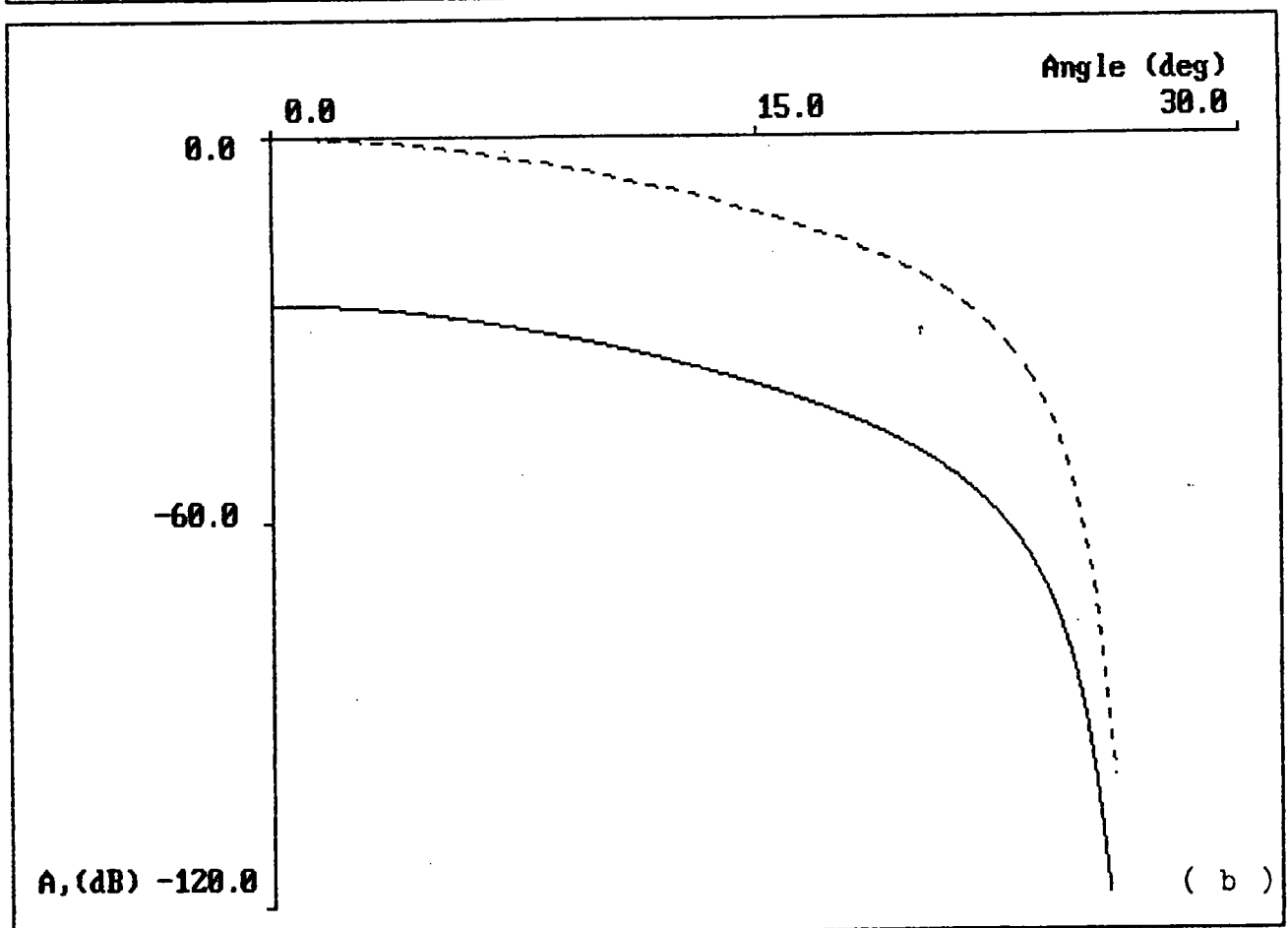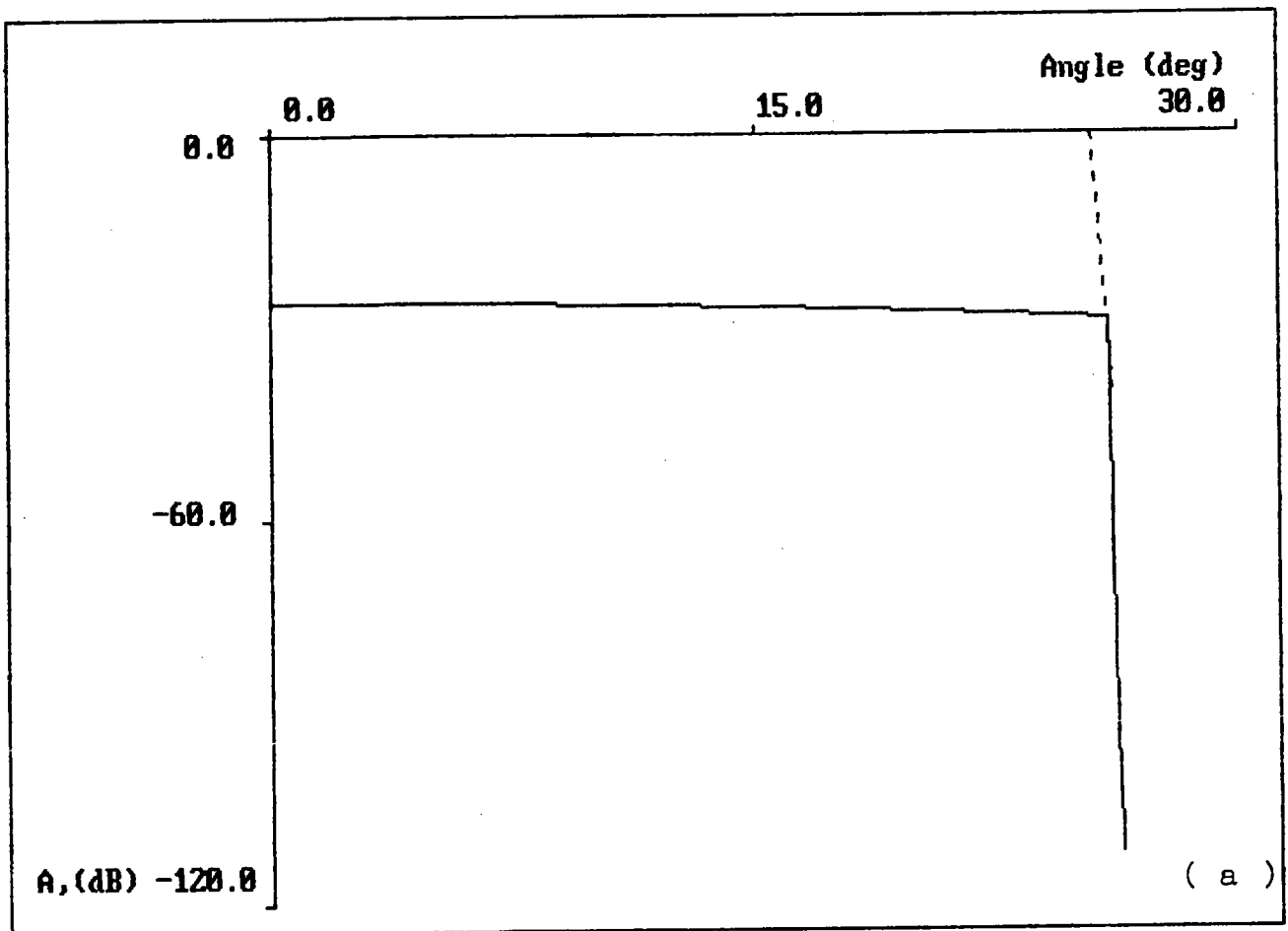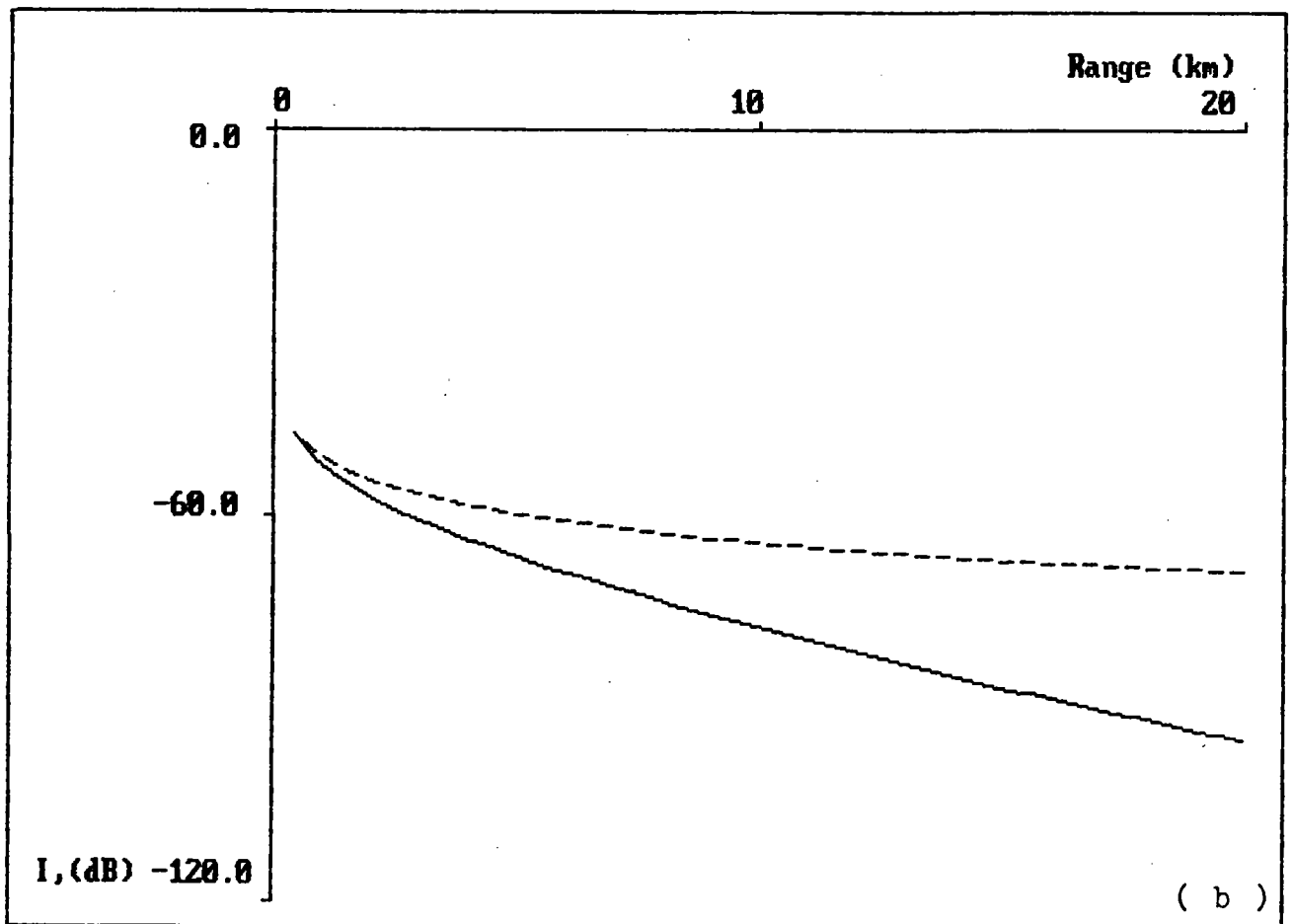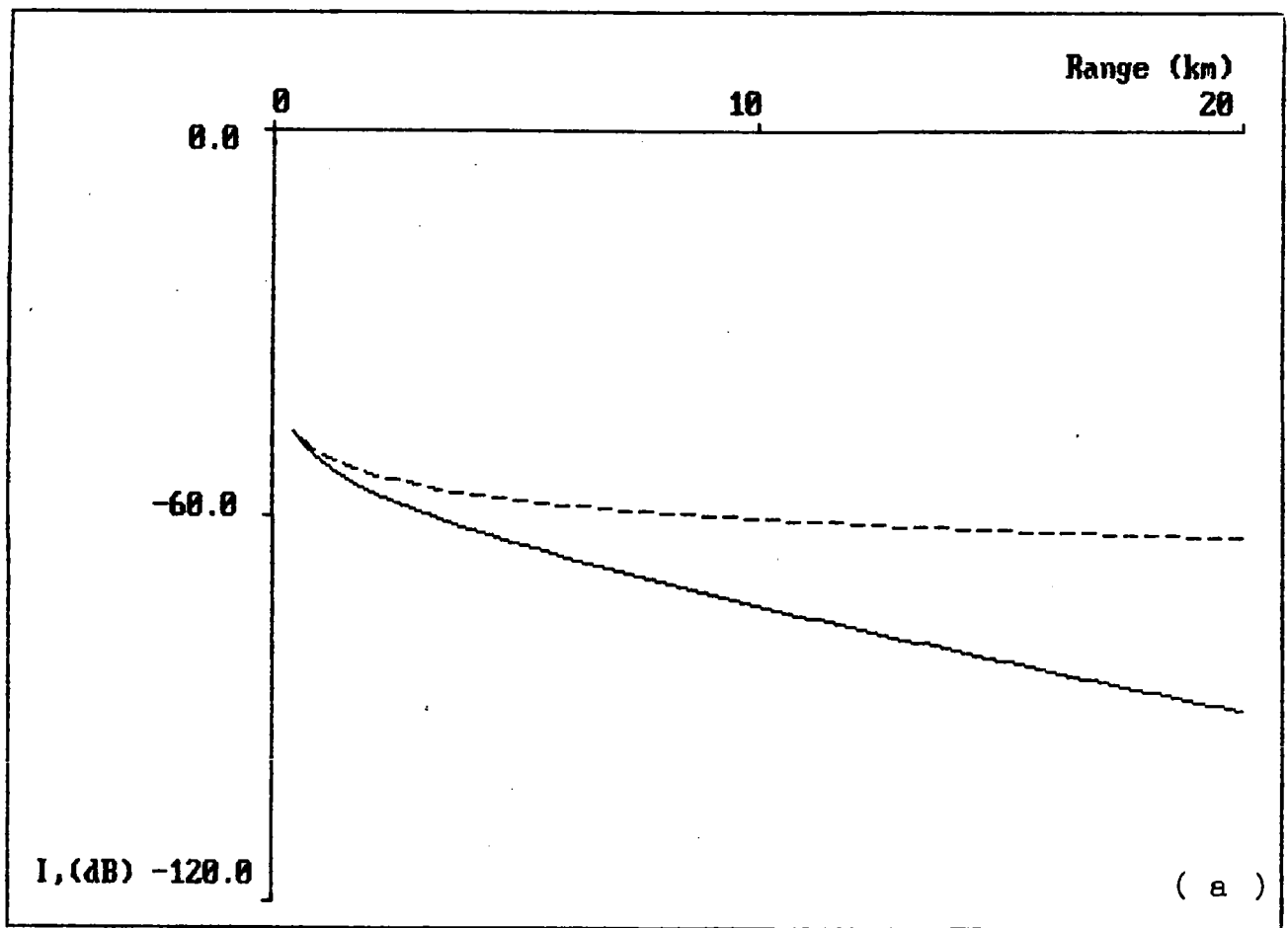
Fig. I.4

Fig. I.5

Fig. I.6

Sound Speed (m/s)

1400   1450   1500

0.0

Source

Receiver

50.0

Depth (m)
100.0

(a)

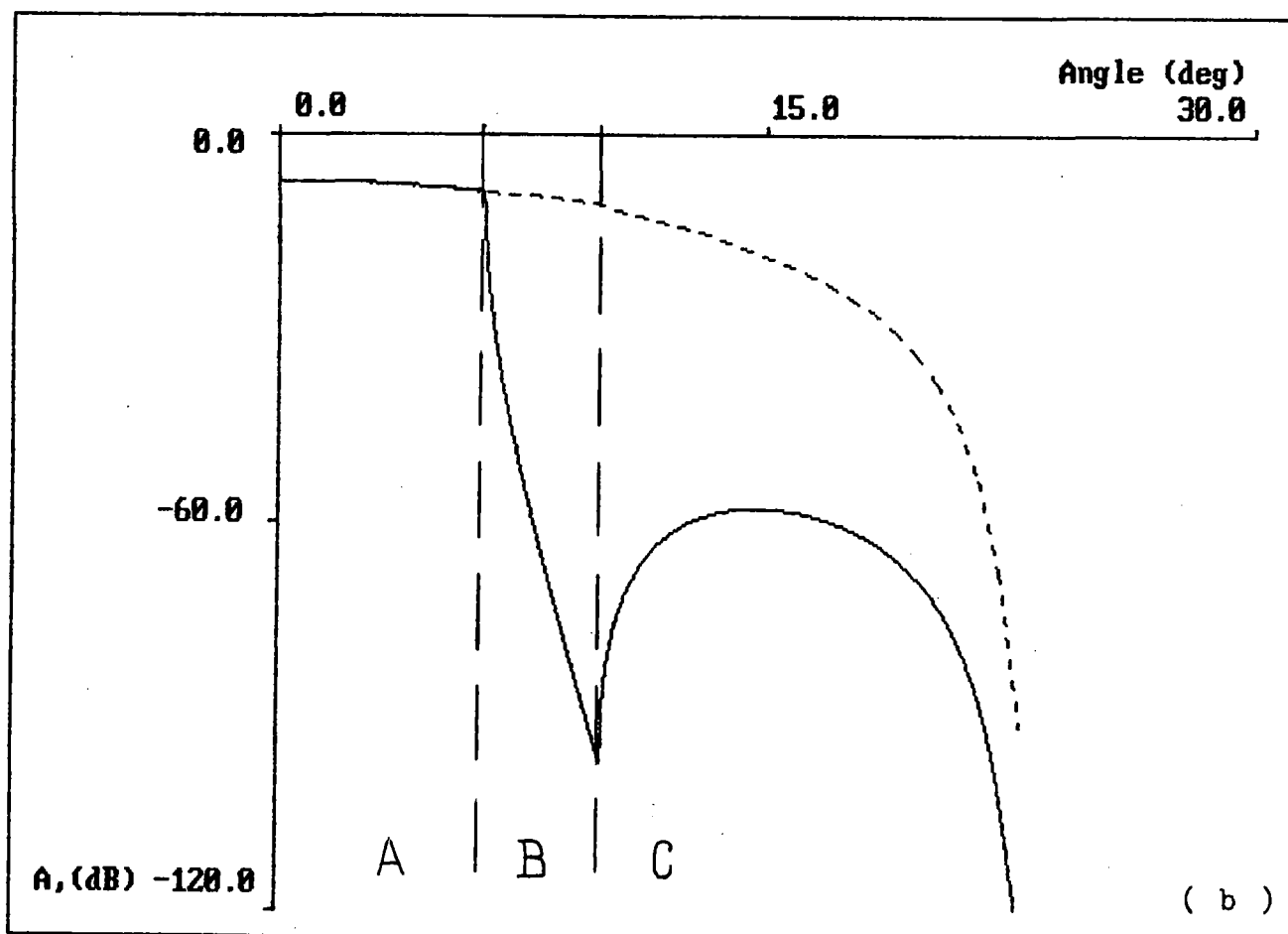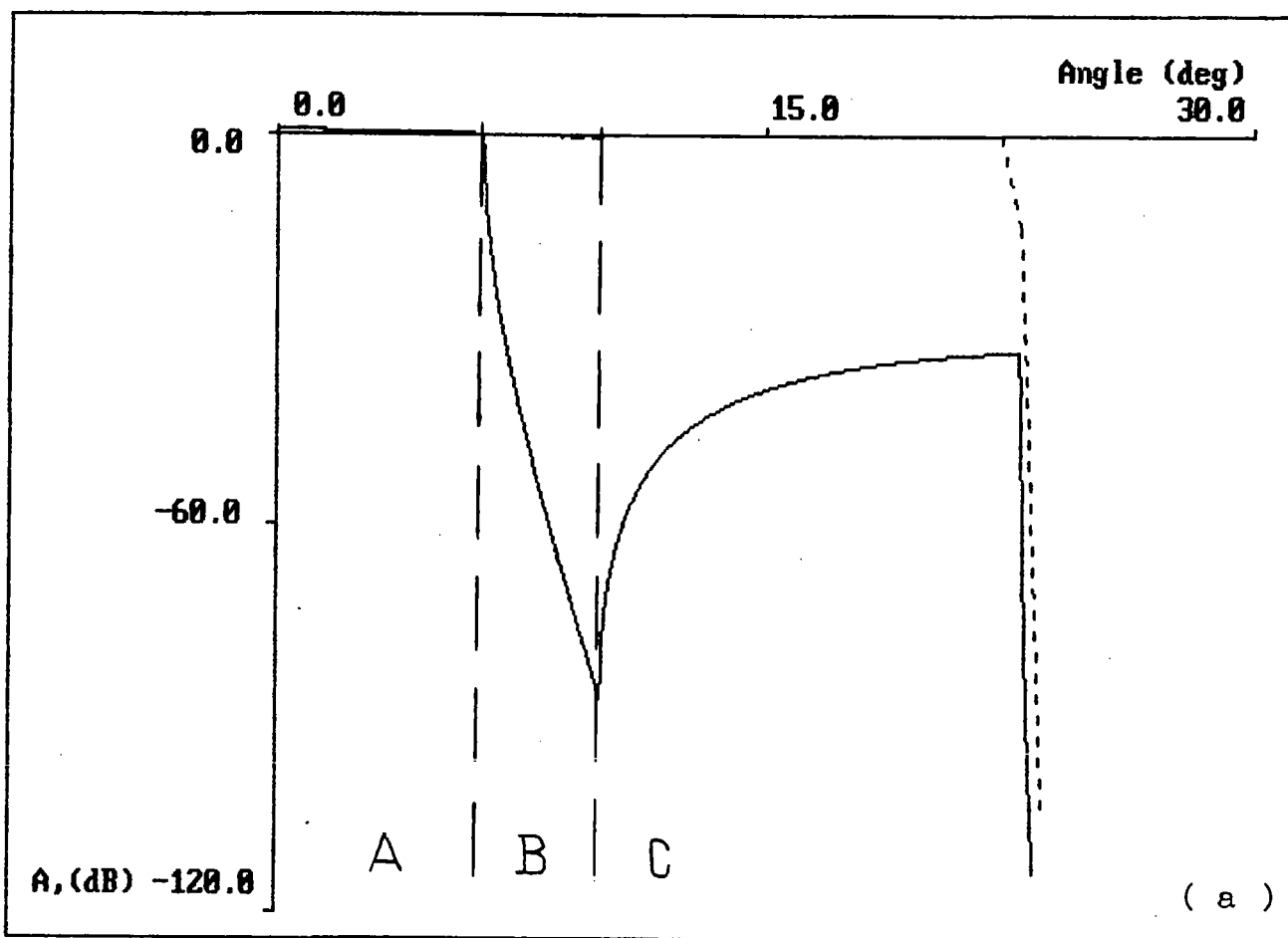C   B

A
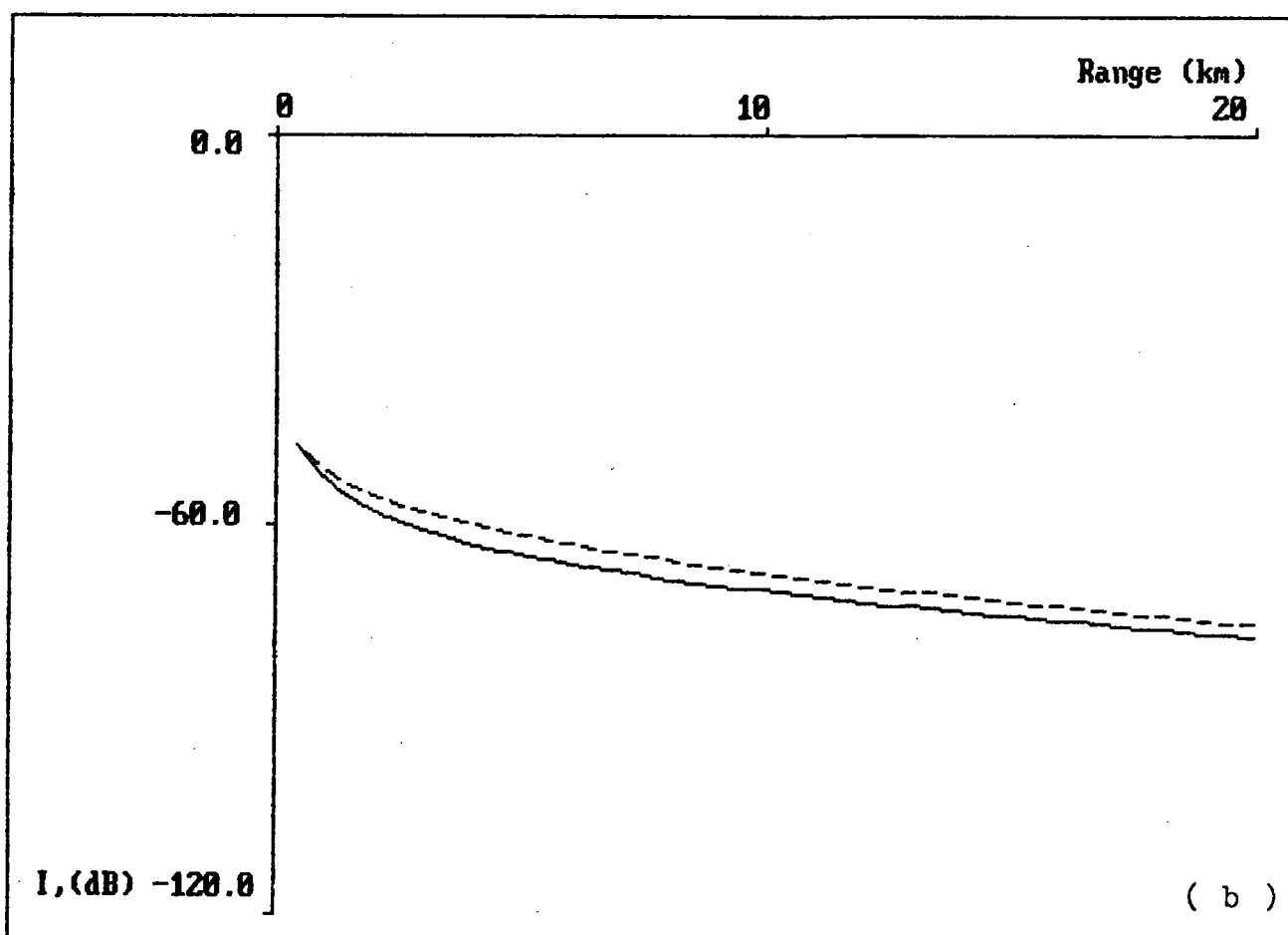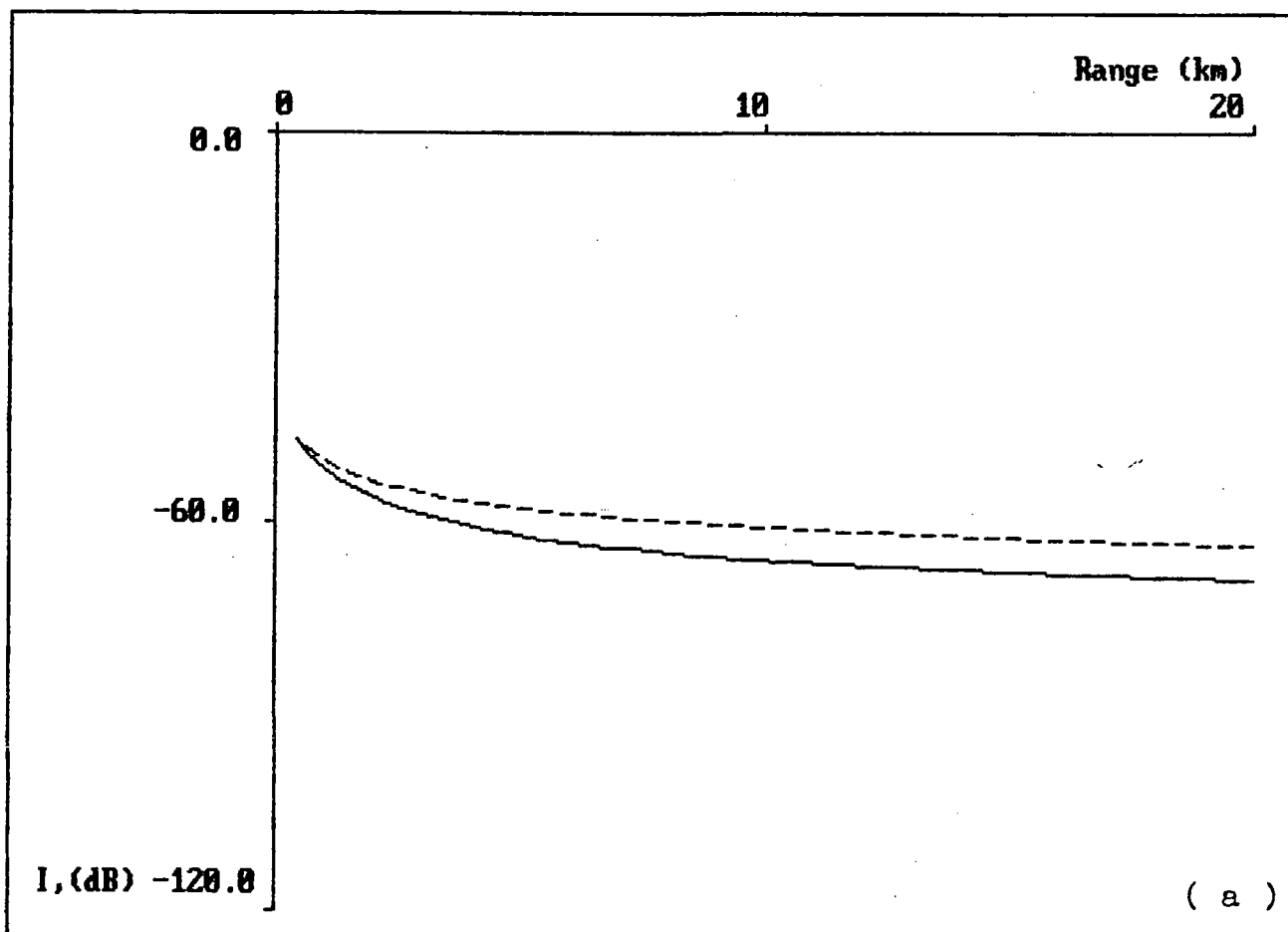
Fig. I.7

(b)
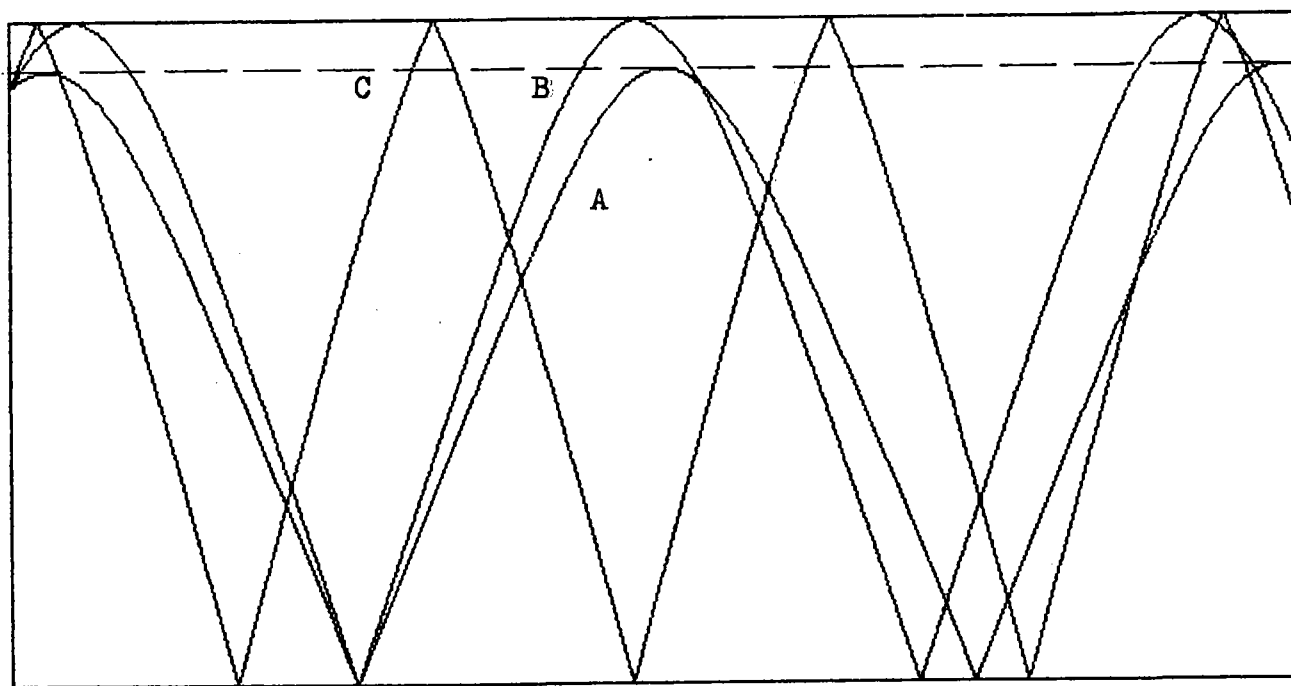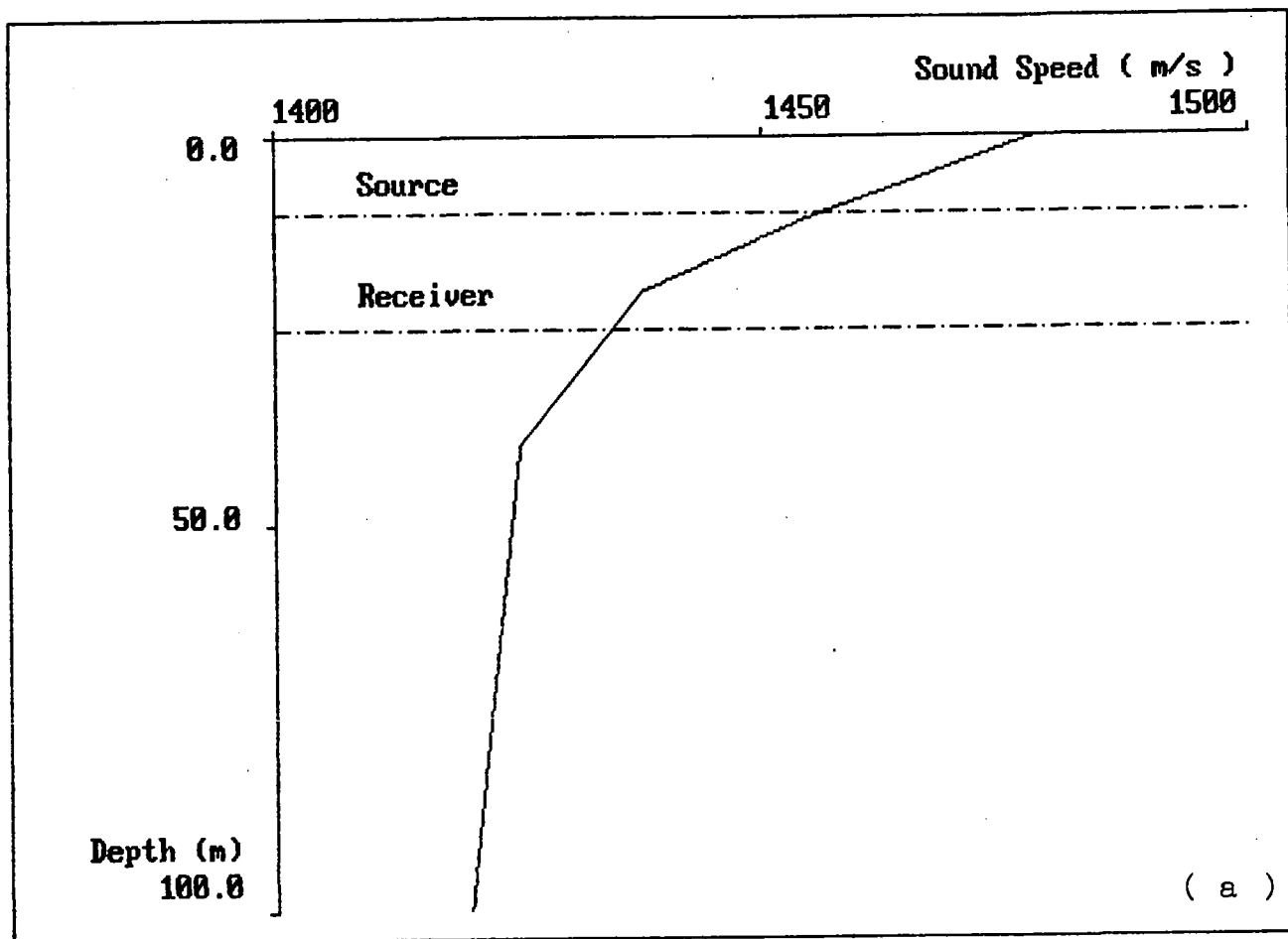
Fig. I.8

Fig. I.9

influence of bottom absorptivity is significant and at rather great values makes the the bubble induced attenuation to be hardly distinguished. Obviously, this effect is concerned with the fact that all the rays which reach the bubble layer have a great inclination at the bottom and due to it are strongly attenuated there. So their contribution to the averaged field intensity is less than for the bottom without absorption. As it is seen from the Fig.1.9 (a) the additional loss due to the bubble layer $\Delta TL \approx 6$ dB, and for the bottom with absorption (Fig.1.9(b)) $\Delta TL \approx 2$dB.

It is seen that for considered models the effect of signal level decrease due to the bubble layer is rather visible. But in general case the bubble induced attenuation depends both on stratification and bottom characteristics. Nevertheless, under some particular conditions of propagation one can hope that the determining of bubbles concentration by measuring transmission loss is possible.

Chapter 2.
Acoustic properties of Lake Ontario

2.1 HYDROLOGY AND SEASONAL EVOLUTION OF TEMPERATURE PROFILES

In order to solve the main problem – the study of the feasibility of determining bubble concentration across Lake Ontario using underderwater acoustic transmission loss it is necessary to introduce the acoustic model of the proposed path, on which experiments will be carried out. This path connects the western tip of Toronto Island (point A) and the mouth of Welland Canal (point B) (Fig 2.1) and it is about 42 km long with the maximum depth along the path 110 m. Path relief (Fig 2.2) is characterized by the inclination angles $\approx$ 3° near Toronto Island and $\approx 1^{\circ}$ near Welland Canal with a rather plane bottom along the path (from 8 km to 32 km).

The waveguide character of the propagation of acoustic waves is determined mainly by the stratification of the sound speed. The seasonal dependence of the sound speed on the depth $c = c(z)$ for various months was calculated using the vertical sections ot the Lake Ontario given by the Scientific Authority Dr.B.Kerman in accordance with the expression [31] :

$$c = 1449.2 + 4.6T - 0.055T^2 + 0.00029T^3 -$$
$$- 35(1.34 - 0.01T) + 0.016z, \qquad (2.1)$$

where c is the sound speed in m/s, T – temperature, z – depth (m). Considering the Fig.2.3, one can see that during the winter months the formation of the isovelocity waveguide canal takes place ($c = const$). With the heating of upper water layers during the warm months the sound speed reaches its maximum value on the lake surface and decreases with the depth. It leads to the formation of the subsurface waveguide. The decrease of temperature of the upper water layers during the fall leads to the decrease of the sound speed gradient in upper layers and to the diffusion of the waveguide . Hence,
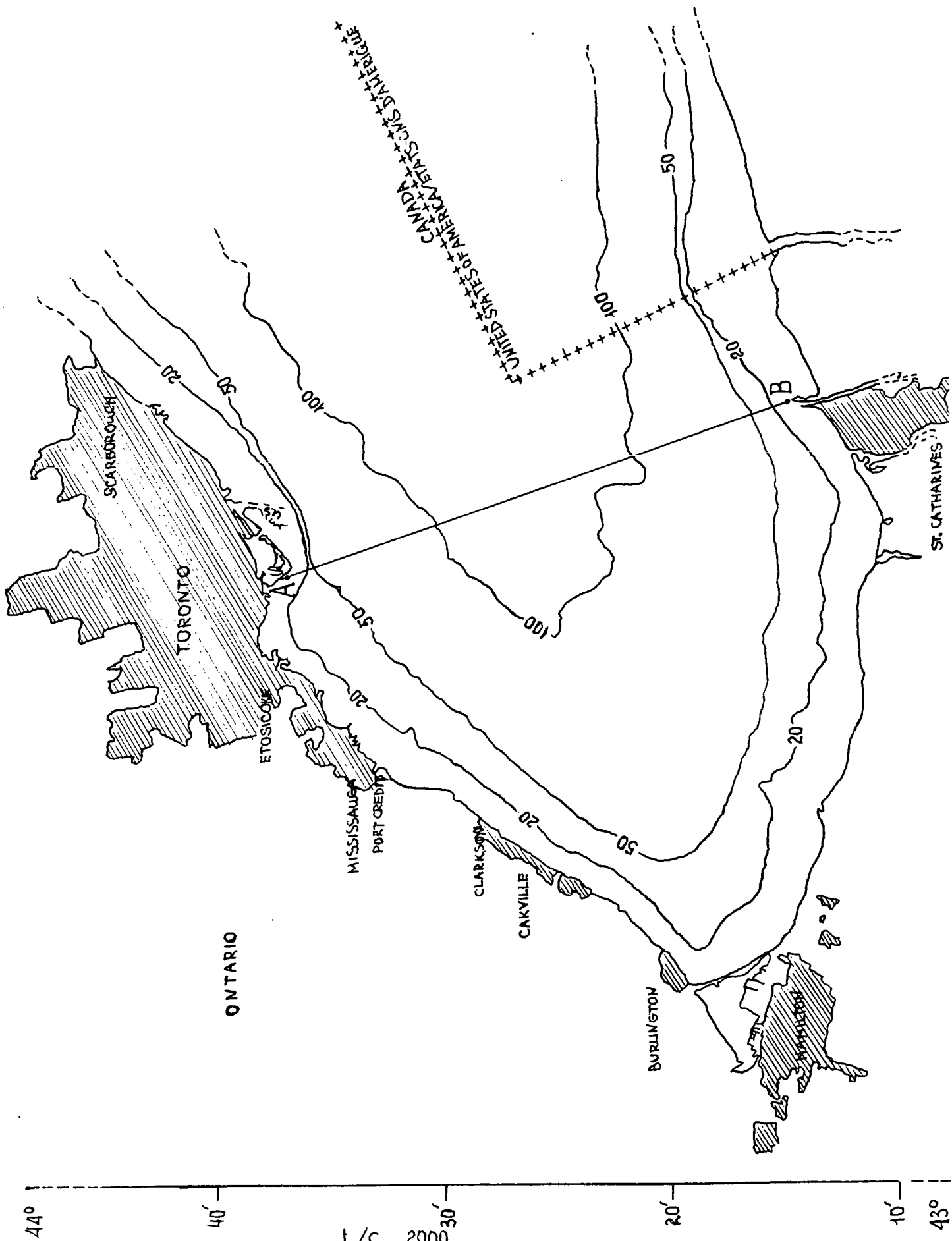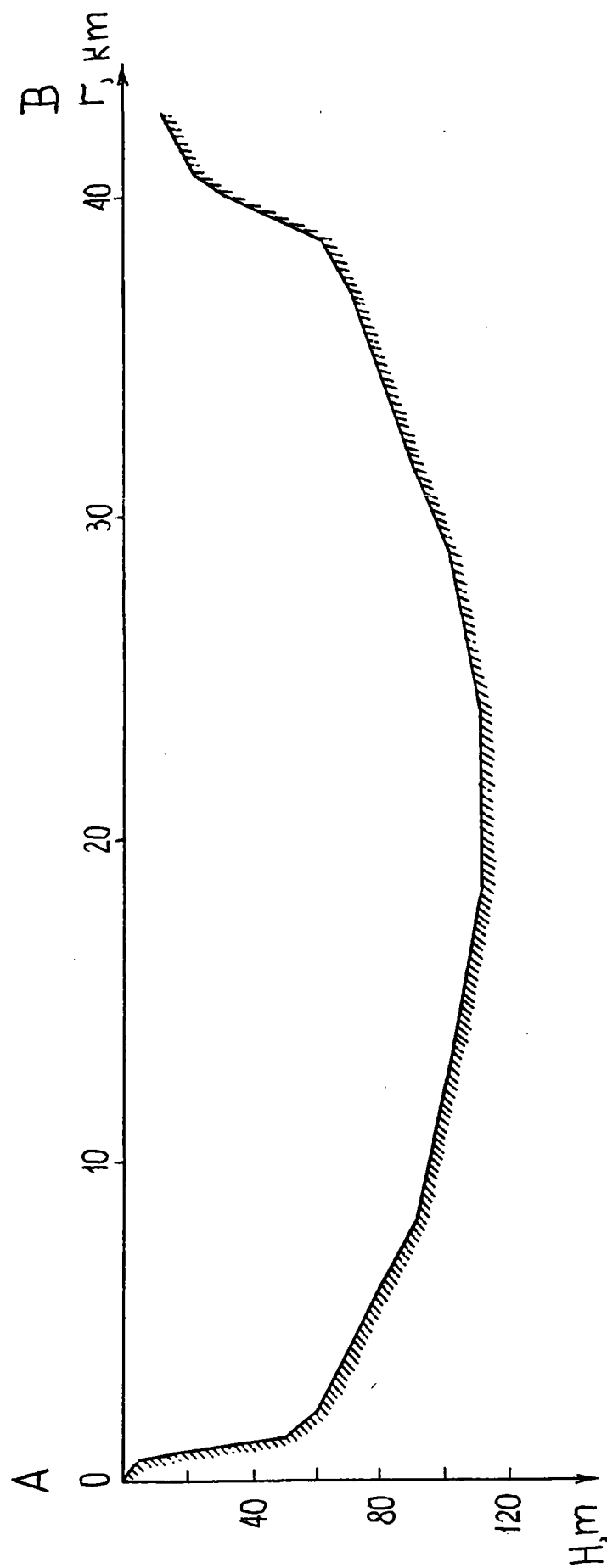
L/C 2000

Fig. 2.I

Fig. 2.2

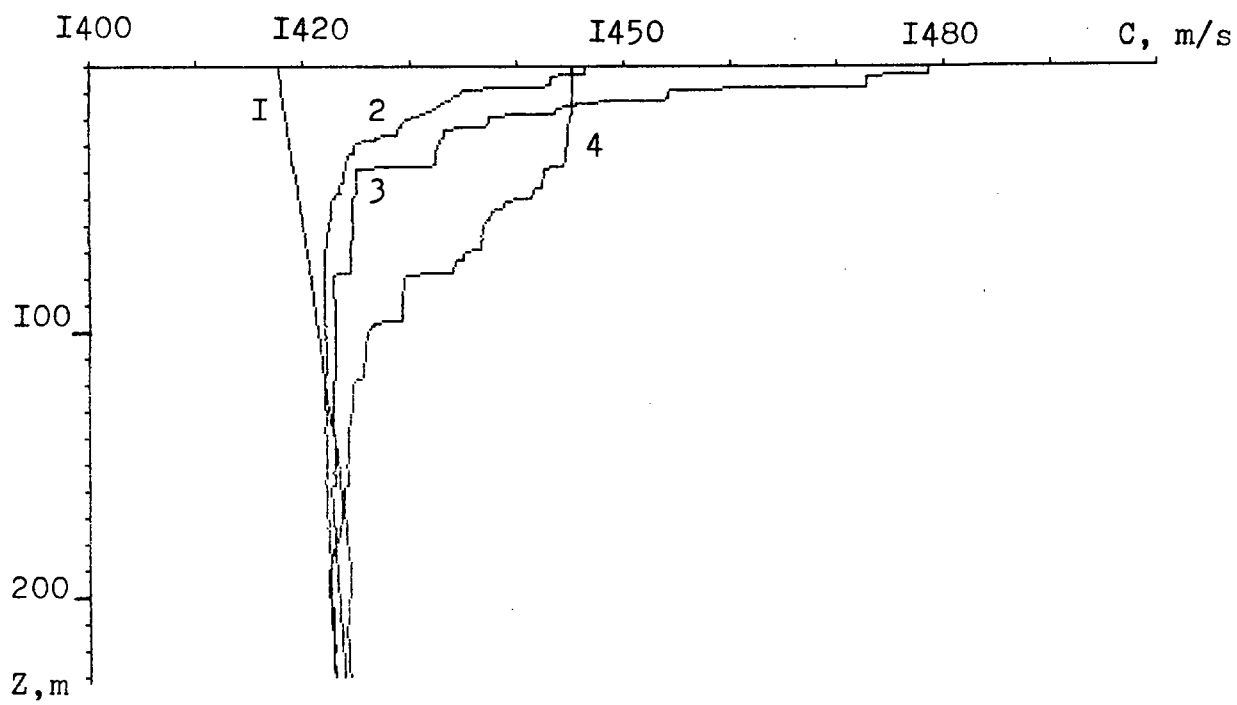Fig. 2.3   Sound speed profile in Lake Ontario.

I - January ,
2 - June ,
3 - July ,
4 - October .

two kinds of stratification can be used for the modelling of the sound propagation:

a) "winter" profile $(c(z) = const)$ during the cold season (isovelocity waveguide)

b) "summer" profile $c = c(z)$ with the maximum value at the surface decreasing with the depth till $z = 50$ m, for $z > 50$ m $c = const$ (subbottom waveguide)

2.2 MAIN MECHANISMS OF SOUND ABSORPTION AND ACOUSTIC MODEL OF BOTTOM

The absorption of the acoustic energy in the water layer and in the lake's bottom should be taken into account for the estimation of the level of an acoustic signal at the path of propagation. The following expression [1] can be used for the absorption coefficient β_w [dB/m] in fresh water

$$\beta_w = 1.64 \times 10^{-4} f^2 / c^3 \quad [\text{ dB/m }] \qquad (2.2)$$

where c is the sound speed (m/s), f - frequency (Hz). It follows from (2.2) that the absorption determined by the shear viscosity in the fresh water at the frequencies less than 10 Hz can be neglected. Thus, the absorption coefficient β_w at 10 kHz is equal to 5.73 $\times 10^{-3}$ dB/km ($c = 1420$ m/s), which leads to the signal decay 0.23dB at the path 40km.

The main mechanism restricting the far sound propagation (side by side with the cylindrical divergence) is the absorption of the acoustic energy in bottom. The information on the structure of the bottom layers in different lake's areas can be obtained from data concerning the upper sediments of Lake Ontario given by the Scientific Authority, which are not, unfortunately, related exactly to the proposed path. The capacity of layers varies considerably and depends on the area. In the generalized geological model four main layers can be singled out:

-Lacustrine A,B (thin layer of the water-satiated clay),

26

-Glaciolacustrine (thickness up to 10 m),
-Drift,
-Bedrock.

Only the three upper layers influences the sound propagation at the frequency band from 100 Hz to 10 kHz, and, as it can be seen from Fig 2.4., the massive Lacustrine layers A,B lays outside the chosen path. Using the data concerning the acoustic properties of sediments [32] the model, comprising the Glaciolacustrine layer 6 m thick laying on the homogeneous half-space (Drift) was chosen (Tab.2.1)

Name	Thickness (m)	Density (kg/m^3)	Sound speed (m/s)	Absorption coefficient η
Glacio-lacustrine	6	1.5×10^3	1470	0.003
Drift		1.8×10^3	1580	0.02

Table 2.1.

where η is the absorption coefficient equal to the ratio between the imaginary and the real part of the wave number. The dependence of the coefficient of reflection $V = V(\chi)$ from this bottom is shown at the Fig 2.5. (a,b) for the frequencies f = 100 Hz and f = 10 kHz. It can be seen that with the increase of the frequency the critical angle χ_* decreases from 23° to 13°, i.e. for the low frequencies (f < 200 Hz) the sound propagation is determined mainly by the half-space and for the frequencies more than 400 Hz the main factor is the upper layer.

But, as it follows from the expression for the average intensity (1.18), the main part of the acoustic energy is concentrated during the propagation on long distances within the angle band $\chi \ll \chi_*$. But for these angles the reflection coefficient is determined by the sound speed difference at the bound. At Fig.2.6(a) the dependence of reflection coefficient on the angle (from 0° to 90°) for the different frequencies

Fig. 2.4

V(χ)

I

0,5

30   (a)   60   χ (deg)

f = Ioo Hz
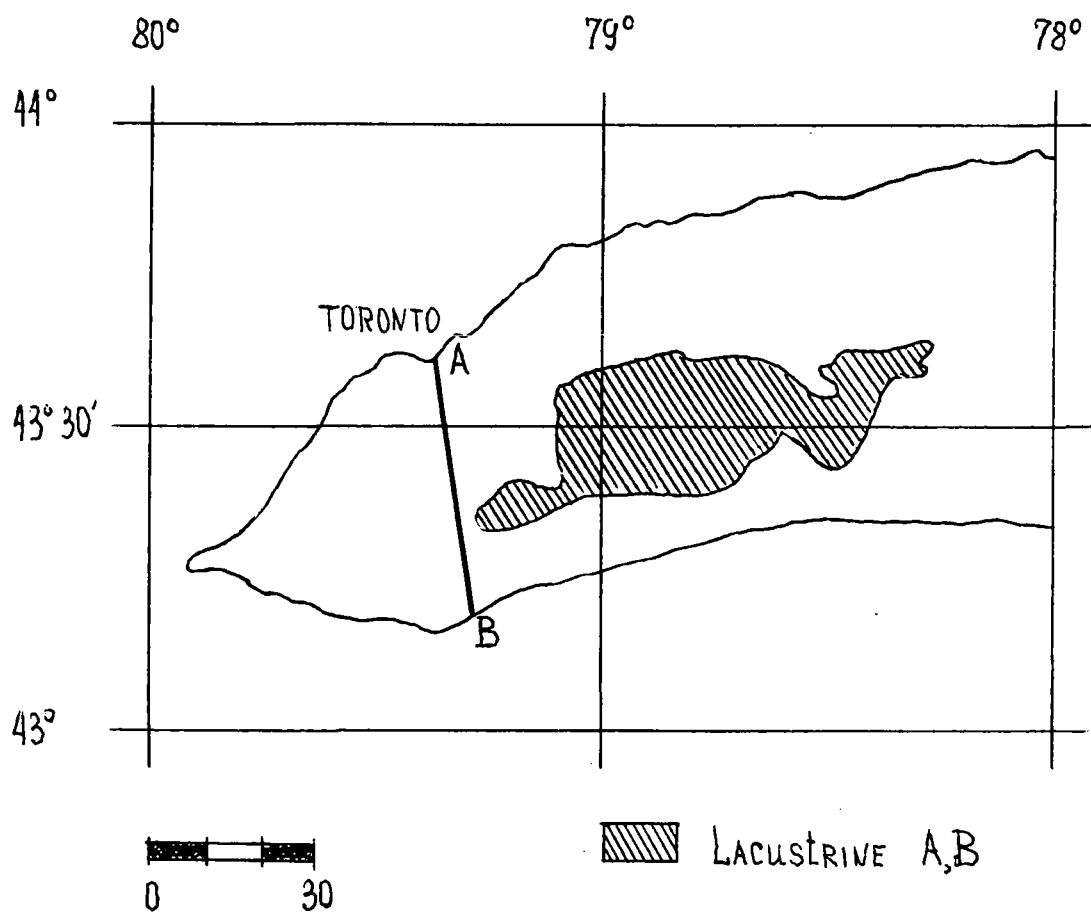
V(χ)
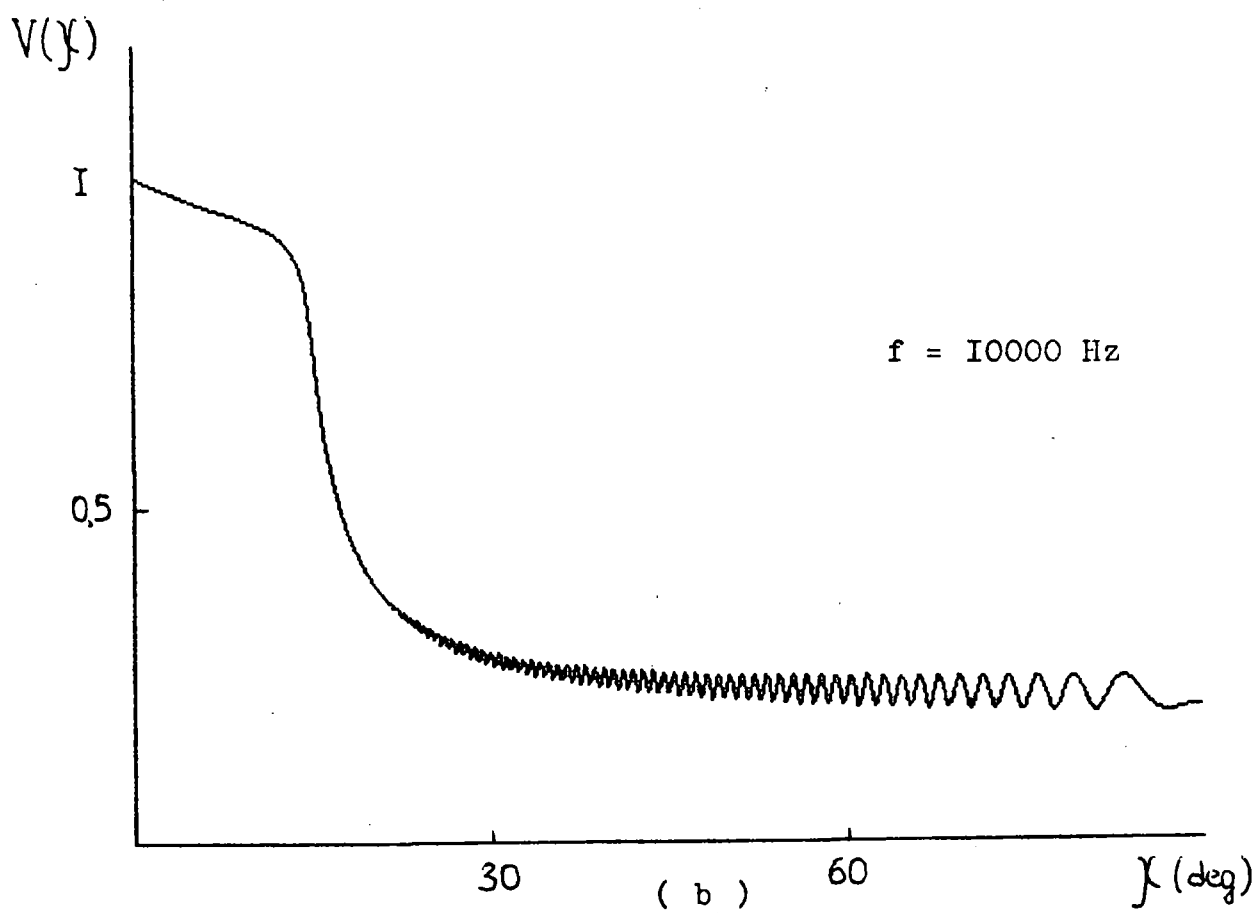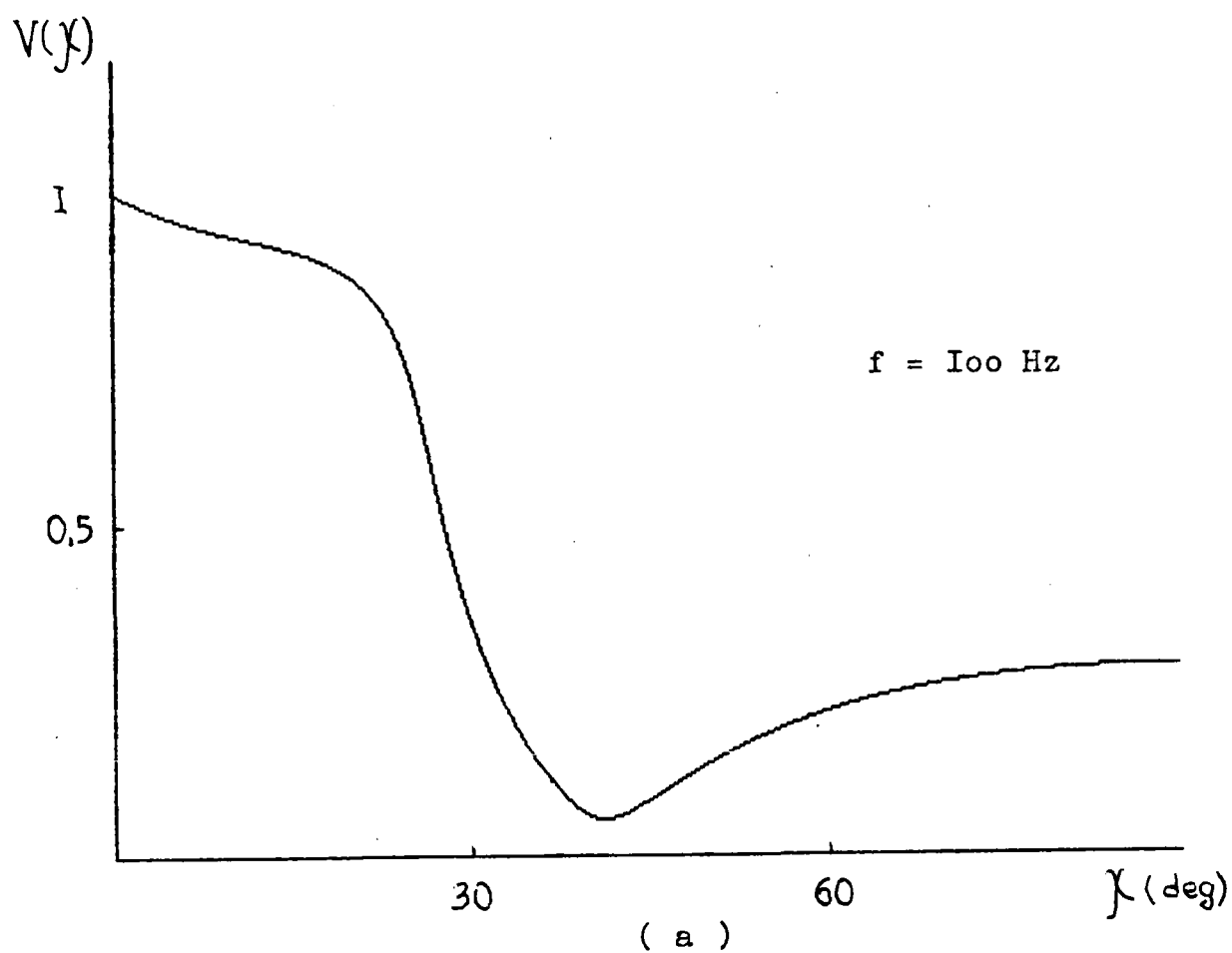
I

0,5

30   (b)   60   χ (deg)

f = I0000 Hz

Fig. 2.5   Bottom reflection coefficient.

29

from 100 Hz to 10000 Hz is shown. As it follows from the figure the reflection coefficient does not depend on the frequency at small angles χ.

It must be noticed that the presence of the upper water-satiated layer of sediments (Lacustrine A, B) might significantly change the bottom reflection coefficient and, hence, the transmission loss at high frequencies. At Fig.2.6(b) the dependence of reflection coefficient for the same angle and frequency ranges is presented for the case of the presence of thin layer of Lacustrine A, B . The thickness of layer is 1 m, sound speed in it c_b = 1425 m/s, its density ρ = 1.4x10^3 kg/m^3 and η = 2x10^{-3}. It is seen, that the reflection coefficient strongly varies at the frequencies f > 800 Hz and almost does not changes at f = 100 Hz. Thus, to determine the transmission loss along the path one needs more exact information about bottom properties.

2.3 ESTIMATES OF NOISE LEVELS
WITHIN DIFFERENT FREQUENCY BANDS

The distant acoustic diagnostics of subsurface bubble layers requires to solve the problem of detection of signal from noise and reverberation. For the frequency range from 100 Hz to 10kHz the ambient noise is the prominent one. Noise, generated by the action of wind on the water surface has been extensively studied and has usually been parametrized as a function of wind speed [35], although the air – sea temperature difference also clearly plays a role [34]. The reassuring factor is the good agreement of noise levels in shallow water with each other and with levels in deep sea in the absence of biological and traffic noise sources, when the only source is a wind [35-38].

The averaged characteristics shown at Fig.2.7 are obtained as the result of selection and averaging of the spectra over the conditions which are presented in Table 2.2.
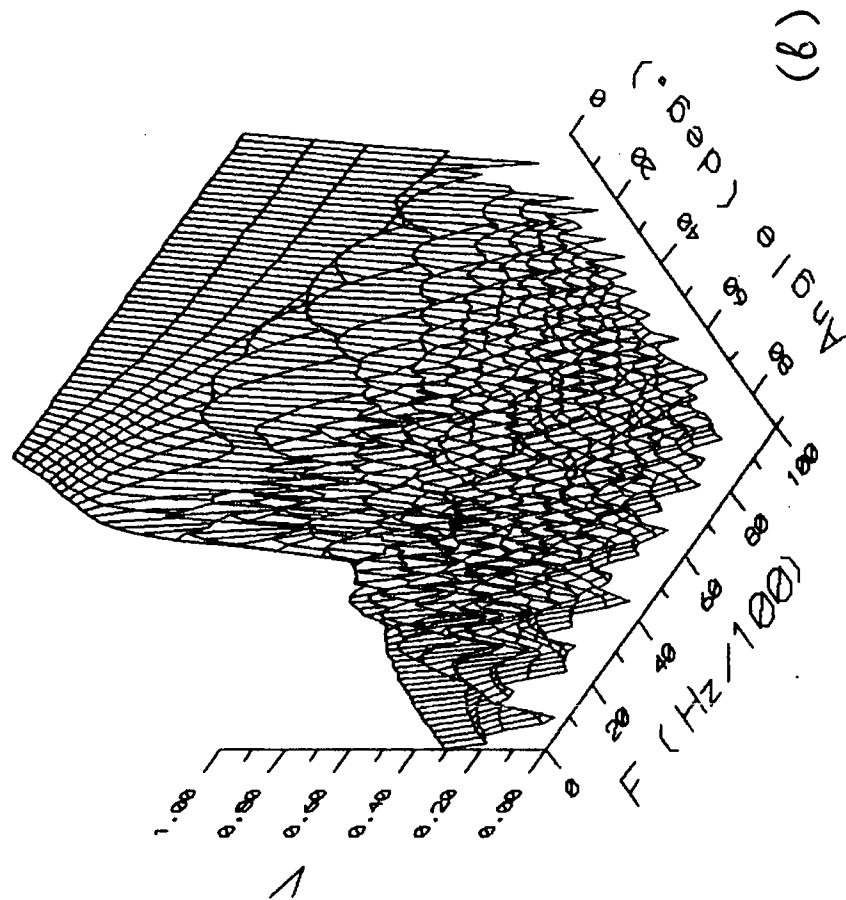
(a)

(b)
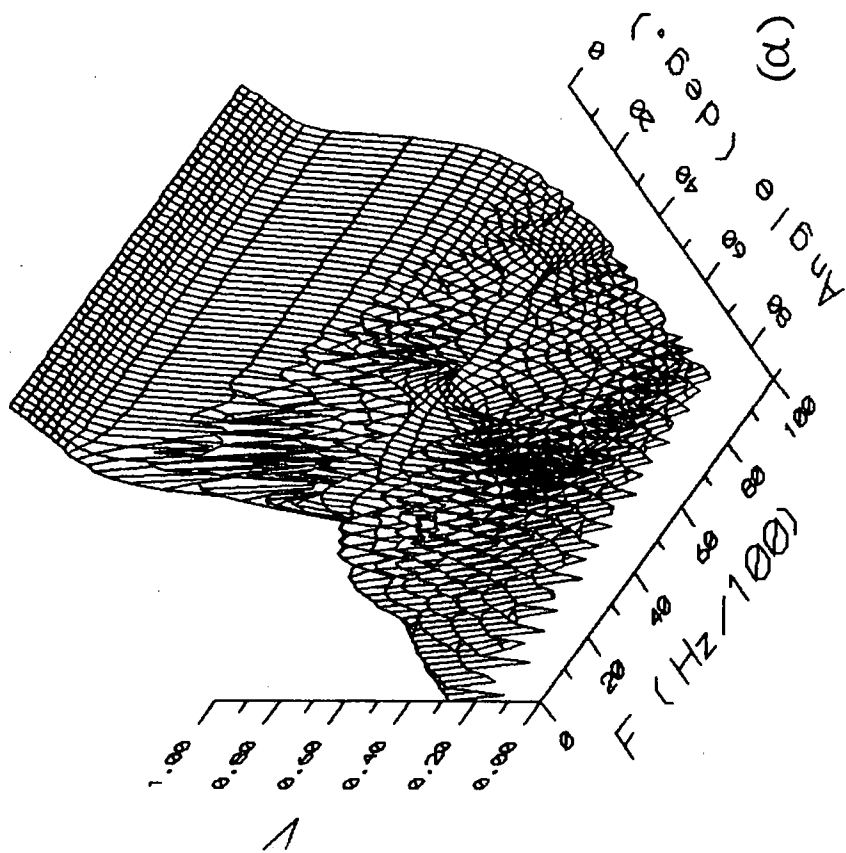
Fig. 2.6
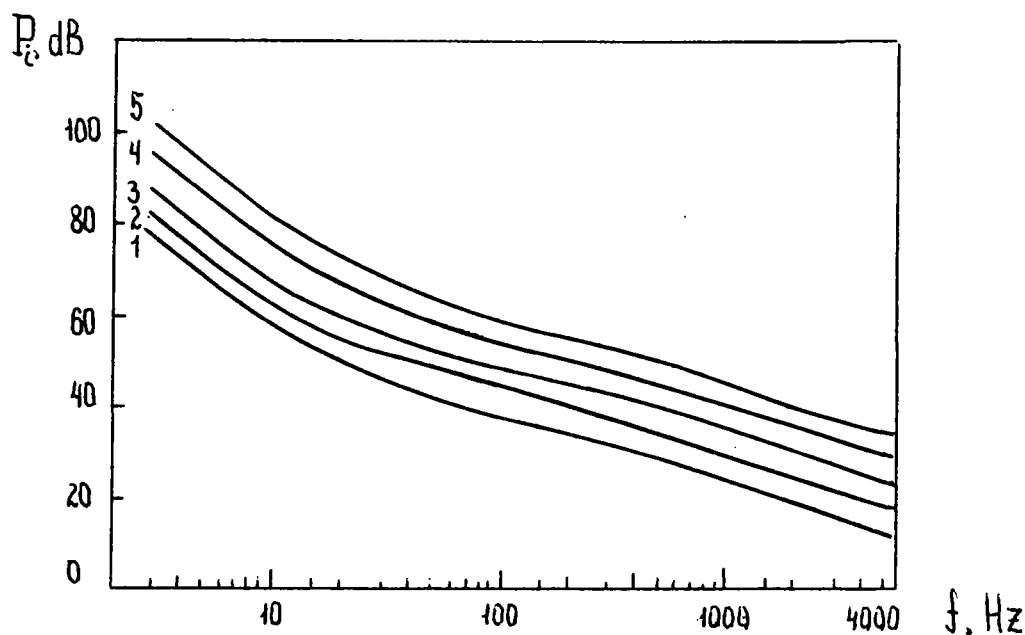
Fig.2.7

No.	Wind speed m/s	Wave height m
1	1.8 - 3.3	0.25 - 0.5
2	3.4 - 5.2	0.5 - 1
3	5.3 - 7.4	0.75 - 1.5
4	7.5 - 9.8	1.25 - 2.5
5	9.9 - 15.2	2 - 5

Table 2.2

Each characteristic is given by the averaging over 80 – 100 frequency spectra. Such figure is convenient for calculation of the threshold level of signals. The general dynamic band of noises (for the frequency range 100 – 10000 Hz) is 60 dB, and for each frequency – about 25 dB, depending on the wind speed. (The noise level (dB) is taken relatively to

2×10^{-5} Pa/Hz$^{1/2}$).

Below the formulae for calculation of noise level in the deep region of an ocean at the constant wind speed up to 20 m/s are represented. These formulae are valid for the frequency range 100 – 10000 Hz and depth of receiver up to 100 m and are obtained by the approximation of spectra shown at Fig.2.7:

$$p_t = 0.18 \, U^{1.5} f_t^{-0.84}$$

$$P = 0.22 \, U^{1.5} \left[\frac{1}{f_1^{0.66}} - \frac{1}{f_2^{0.66}} \right]^{1/2}, \qquad (\, 2.3 \,)$$

where p_t is the sound pressure within the frequency band 1 Hz at the frequency f_t, P (bar) – the sound pressure in the given frequency band from f_1 to f_2, U – the average wind speed.

In conclusion it must be mentioned, that the noise level at Lake Ontario within the used frequency range might increase because of traffic noises (at the low frequencies up to 400 Hz) and due to biological noises (at the all frequencies), but we have no any information about the sources of such noises in Lake Ontario.

Chapter 3.
SOUND FIELD AND TRANSMISSION LOSS IN LAKE ONTARIO

3.1 METHODS OF MATHEMATICAL MODELLING OF SOUND
PROPAGATION IN WAVEGUIDES (BRIEF REVIEW)

The most of papers about numerical simulation of sound propagation are concerned the ocean acoustics. Because of it in this chapter we use the term "ocean" which means a natural water body, where sound speed varies with depth and range and the structure and characteristics of bottom are real. Here we consider the time-independent model without fluctuations of sound speed, of boundaries and any random effects.

When modelling the sound propagation we suppose ocean to be a layer of liquid, settled down on an elastic medium. The liquid is being completely described by functions of its density $\rho_o(\vec{r})$ and sound speed in it $c(\vec{r})$. The elastic medium is described by density $\rho_1(\vec{r})$ and by Lame parameters $\lambda(\vec{r})$, $\mu(\vec{r})$, which allows to calculate the velocities of longitudinal c_l and transverse c_t waves using the well known equations [39]

$$c_l(\vec{r}) = \left[\frac{\lambda + 2\mu}{\rho_1} \right]^{1/2} , \quad c_t(\vec{r}) = (\mu / \rho_1)^{1/2} .$$

The equations which describe the acoustic oscillations and correspondent boundary conditions are presented in [28,39]. It must be noticed that there are some difficulties in solving the general problem. However, in the most of particular cases one can suppose density to be constant ($\rho_o(\vec{r}) = const$) and describe the ocean as a cylindrically symmetric medium with vertical axis z through the source , neglecting the azimuthal scattering. Moreover, because the depth of wave penetrating into the bottom is proportional to the wavelength, at the frequencies $f > 100$ Hz one can neglect

the influence of shear waves, due to their low velocity in upper layer of sediments.

Then, taking into account all these assumptions the problem is reduced to the solving of following wave equation for the acoustic pressure $p = p(z,r)$ [28]:

$$\frac{1}{r}\frac{\partial}{\partial r}\left[r\frac{\partial p}{\partial r}\right] + \frac{\partial^2 p}{\partial z^2} + k^2(z,r)\,p = \frac{\delta(r)\delta(z-z_o)}{2\pi r} \qquad (3.1)$$

with the condition of radiation

$$p(z,r)\Big|_{z,r\to\infty} \to 0 \qquad (3.2)$$

and the boundary conditions

$$p(0,r) = 0\;,\quad [\,p\,]\Big|_{z=H(r)} = [\,v_n\,]\Big|_{z=H(r)} = 0\;. \qquad (3.3)$$

Here z_o is a depth of source , $\vec{v}$ is the velocity of particle oscillations in liquid, [ ] means the continuity of variables. The absorption is introduced as the imaginary part of the sound speed c. Below we some basic methods to solve the problem (3.1 - 3.3).

The wave theory.

The wave theory gives the exact solution of the problem for the case of range - independent waveguide. The solution of wave equation (3.1) might be found using the separation of variables. The sound field can be represented as [40]:

$$p(z,r) = \frac{1}{4\pi}\int_{\mathbb{C}} G(\,z,\,z_o,\,\xi\,)\,H_0^{(1)}(\xi r)\,\xi\,d\xi\;, \qquad (3.4)$$

where G is the function, which satisfies the one-dimensional Helmholtz equation, $H_0^{(1)}(\xi r)$ – the zeroth - order Hankel function of first kind and $\mathbb{C}$ – the integration contour on the complex ξ-plane, which includes all the singularities of G.

In this case the sound field might be obtained as a sum of residues, which correspond to the discrete eigenvalues and the integral taken on the continuous part of the spectrum [40, 41].

Neglecting the contribution of continuous spectrum at the long distances and using the asymptotic representation of $H_0^{(1)}$, we obtain field as the following superposition of normal waves [28]:

$$p(z,r) = \sqrt{2\pi} \sum_n \frac{\psi_n(z_0)\psi_n(z)}{\sqrt{\xi_n r}} exp \left(i\xi_n r - \frac{i\pi}{4} \right) \quad (3.5)$$

where ξ_n and ψ_n - eigenvalue and eigenfunction which might be found from the following equations :

$$\frac{d^2\psi_n}{dz^2} + \left(k^2(z) - \xi_n^2 \right) \psi = 0, \quad (3.6)$$

$$\psi(0) = 0, \quad (3.7)$$

$$\left[\frac{d\psi_n}{dz} + Q(\xi_n) \psi \right]\Bigg|_{z=H} = 0 . \quad (3.8)$$

Here, Q is the input admittance of the bottom, which might be find out for the particular models of bottom using recurrent sequences.

Different methods for numerical solving of the problem (3.6) - (3.8) are reviewed in [41,42]. Moreover, in [41] the method of the calculation of sound field in a layered ocean, based on the direct numerical estimation of integral field representation (3.4) is introduced (FFP - Fast Field Program).

As it was mentioned above, the method of normal waves fails in of range-dependent waveguide. Furthermore, it is not the very effective one at high frequencies, when the number of propagating waves is great.

To describe the field within a framework of wave theory in the case of weakly range - dependent waveguide one can use

36

the adiabatic approach [29]:

$$p(z,r) = \sqrt{2\pi} \sum_n \frac{\phi_n(z_o,0)\phi_n(z,r)}{\sqrt{\xi_n(r)\ r}} \ exp(i\int_0^r \xi_n(r)dr - \frac{i\pi}{4}\ ).\quad (\ 3.9\ )$$

There the range dependence of the ocean's acoustic properties and its boundaries is taken into account by dividing this waveguide into range-independent segments. Then, eigenvalue ξ_n and eigenfunction ϕ_n are determined for each segment and might be approximated for an arbitrary range r (method of cross sections).

The parabolic equation method.

The parabolic equation (PE) method was introduced in underwater acoustics community by Tappert [43]. One of the advantages of the PE models is theirs ability to handle range − dependent environments. Moreover, because these approximation yield equations that have only first derivatives in range, they offer significant computational advantages over other (albeit more exact) solutions of full wave equation (3.1). The transition from this elliptic wave equation (3.1) (boundary value problem) to the one − way wave equation (initial value problem) could be made using the following substitution [44]:

$$p(z,r) = U(z,r)\ H_o^{(1)}(\ k_o\ r\ ),\qquad (\ 3.10\ )$$

where $U(z,r)$ is the slowly varying function (the envelope).

Making this substitution and using the farfield asymptotic representation of $H_o^{(1)}$ one can split the resultant equation into two terms, which yield incoming and outgoing waves. Then neglecting incoming waves we obtain :

$$\left[\frac{\partial}{\partial r} + ik_o[\ 1 - (1+\mathcal{L})^{1/2}\ ]\right] U(r,z) = 0,\quad (\ 3.11\ )$$

where $\qquad \mathcal{L} = k_o^{-2}\ (\ \partial^2/\partial z^2 + k^2(z,r) - k_o^2\ ).$

37

Different approximations to the square root operator $(1+\mathcal{L})^{1/2}$ produce different PEs. The standard PE is obtained by approximation of the square root operator by a two-term Taylor series expansion:

$$\frac{\partial U(z,r)}{\partial r} = \frac{i}{2k_o} \left\{ \frac{\partial^2}{\partial z^2} + k^2(z,r) - k_o^2 \right\} U \quad . \quad (\ 3.12\ )$$

McDaniel [45] analyzed the standard PE within the framework of normal mode theory and found that this approximation introduced phase errors for individual modes, but that the mode amplitudes were correct. The standart PE is valid for angles of propagation up to about 10 deg.

The use of more exact approximations to the square root $(1+\mathcal{L})^{1/2}$ allows to extend the area of PE's applicability as it is shown in the Table 3.1 :

$(1+\mathcal{L})^{1/2}$		
$1 + \mathcal{L}/2$	$10°$	Tappert [43]
$1 + \mathcal{L}/2 - \mathcal{L}^2/8$	$20°$	Mary [46]
$(\ 1+3\ \mathcal{L}/4\ )/(\ 1 + \mathcal{L}/4\ )$	$23°$	Claerbout[47]
$(\ a_o + a_1\mathcal{L}\ )/(\ 1 + b_1\mathcal{L}\ )$	$40°$	Green [48]
$(\ a_o + a_1\mathcal{L} + a_2\mathcal{L}^2)/(\ 1 + b_1\mathcal{L} + b_2\mathcal{L}^2)$	$67°$	Knightly [49]
$(\ a_o + a_1\mathcal{L} + a_2\mathcal{L}^2 + a_3\mathcal{L}^3)/(\ 1 + b_1\mathcal{L} + b_2\mathcal{L}^2 + b_3\mathcal{L}^2)$	$89°$	Vefring [44]

Table 3.1

However, the rising of precision of the approximation leads to the increase of numerical algorithm's complicity and requires much time for the calculation. So when solving particular problems, one has to make a compromise between precision and these two factors.

Among all numerical methods of solving PEs three main direction must be distinguished [41]:
1. Split - step Fourier algorithm.
2. Ordinary - Differential - Equation (ODE) method.
3. Implicit Finite - Difference (IFD) method.

Each method has both advantages and shortcomings. Split - step algorithm gives a unconditionally stable numerical solution, but is the effective one only when using FFT processor. The IFD method is stable as well, but at the every range step requires to inverse the high-order complex matrix. ODE methods are of high performance, but are unstable in some cases.

As it was noticed, the main advantage of the PE method is that it might be used in a case of range - dependent duct. This method automatically takes into account the interaction between normal waves and describes exactly the diffraction effects.

However, because the amount of calculations increases like f^2, the use of this method at high frequencies is rather unexpedient.

The ray theory.

The ray approach is the high-frequency approximation for the solving of (3.1). Equations of the ray theory might be obtained from Helmholtz equation by means of the following substitution :

$$p(\vec{r}) = A(\vec{r})exp(\iota k_o W(\vec{r})), \qquad (3.13)$$

where A and $k_o W$ are the amplitude and the phase of the wave respectively, and k_o is the reference wave number $k_o = \omega/c_o$. In

this case we have the following equations [28]:

$$(\nabla W)^2 = (c_o/c(\vec{r}))^2 , \qquad (3.14)$$

$$2 \nabla A \nabla W + A \nabla W = 0 . \qquad (3.15)$$

Equation (3.14) determines the geometry of rays, i.e. of lines which are perpendicular to phase surfaces $W = const$. And equation (3.15) gives the amplitude of wave.

The process of sound field calculation within the framework of ray approach might be divided into the following parts :

1. The determination of the ray trajectories which reach the receiver (two - point ray tracing). To solve this problem the algorithms based on the special methods of approximation of the sound profile are the most effective ones. In such methods the shape of the finite parts of rays might be found analytically. It makes the computations more fast [42].
2. The calculation of the optical ray lengths W_n.
3. The calculation of the field amplitude A_n on the rays at the point of receiver, taking into account the energy flow conservation within ray tubes, the reflection coefficient of bottom, the change of phase at the caustics, etc.
4. The summing of contributions of all the rays which reach the point of receiver $- A_n exp(ik_o W_n)$.

The main difficulties of the ray method are concerned with the two - point ray tracing problem. Moreover, it fails on the singular regions (the vicinity of caustics, critical regions, the transition regions between the illuminated and shadow zones, etc.).

To calculate the averaged intensity of sound field in the range dependent waveguide one can use the method of adiabatic invariant [29,30].

Averaging the equation (3.9) over the range and using the WKB approximation for eigenvalue and eigenfunction [50] one can obtain the following expression :
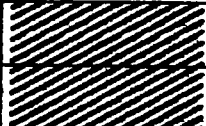
$$< I >_{(z,r)} = < pp^* > = \frac{4}{r} \int_0^{\pi/2} \frac{exp(-2 \int_0^r \beta(r)dr)}{tg \; \chi_o \; D(\chi_o,0)} \; d\chi \; , \quad (3.17)$$
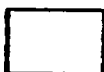
where

$$\beta(r) = \frac{ln \; |V(\chi,r)|}{D(\chi,r)} \; ,$$
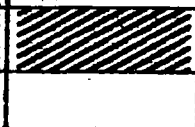
χ_o is the departure grazing angle of ray at the source, χ is the inclination (grazing angle) at the point of receiver, $D(\chi,r)$ — the cycle length of a ray, $V(\chi,r)$ — the reflection coefficient of the bottom. The angles χ_o and χ are connected by phase integral of WKB approximation [50].

The conclusions about the expedience of the use of these methods for range — dependent and —independent waveguides are presented in the Table 3.2 for low (LF) and high (HF) frequencies.

METHOD	range – independent		range – dependent	
	LF	HF	LF	HF
Normal Modes	////		////		
PE	////		////	////	////
Ray		////		////

☐ — inapplicable   ▨ — applicable

▨ — applicable, but requires a lot of calculations

Table 3.2

3.2 SOUND FIELD DISTRIBUTION
ALONG THE RANGE - INDEPENDENT WAVEGUIDES

The comparison of different numerical methods for the calculation of acoustic fields has been carried out for two layered models ("winter" and "summer" models) of the plane waveguide (parameters of both models are shown at Fig.3.1, 3.2). The first model corresponds to the typical winter conditions of sound propagation in the region of proposed path, the second one - to the summer conditions (see Chapter 2.2). Three programs of sound field calculation are used. These programs are based on (1) method of normal waves [51], (2) method of high - angle PE [52] and (3) method of ray adiabatic invariant (see Appendix A).

At Fig. 3.3 and 3.4 the range dependencies of transmission loss (TL) computed by these programs for both models of waveguide are presented. Source frequency f = 200 Hz, depth of source z_o = 75 m, depth of receiver z = 50 m . At this frequency 12 modes with phase velocity $v_n < c_2$ (sound speed in the bottom half-space) propagates in the waveguide. However, the modes of high order are being attenuated greatly, so at the long distances the field structure becomes rather simple. As it is seen from the figures, the normal waves .method (coherent model) and the method of high-angle PE show approximately the same results.

Because the ray invariant method allows to determine only the average (over z and r) field we compare it with incoherent model of normal waves method. Within the framework of incoherent model the amplitudes of particular modes are summed without taking into account the interference items, so
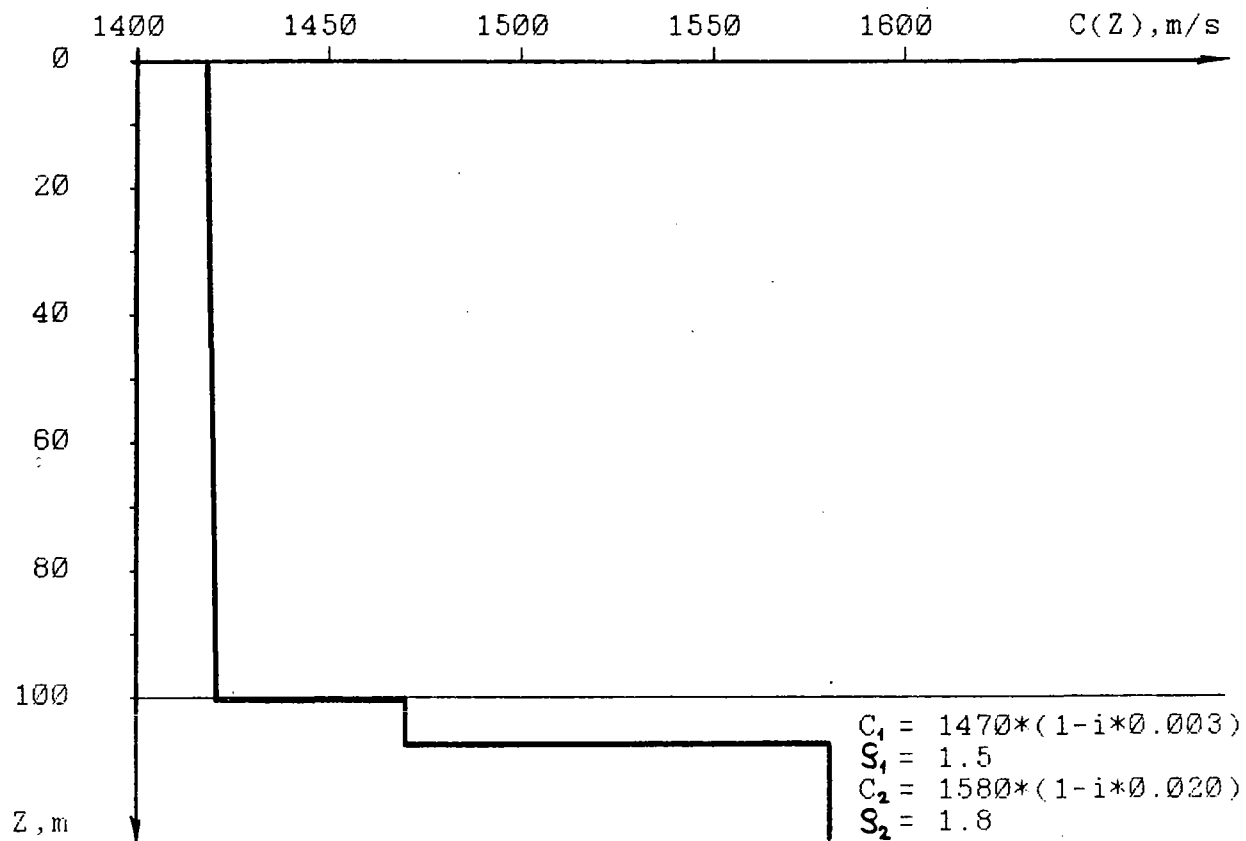
$$C_1 = 1470*(1-i*0.003)$$
$$S_1 = 1.5$$
$$C_2 = 1580*(1-i*0.020)$$
$$S_2 = 1.8$$

Fig. 3.1 "Winter" waveguide model.

$$C_1 = 1470*(1-i*0.003)$$
$$S_1 = 1.5$$
$$C_2 = 1580*(1-i*0.020)$$
$$S_2 = 1.8$$
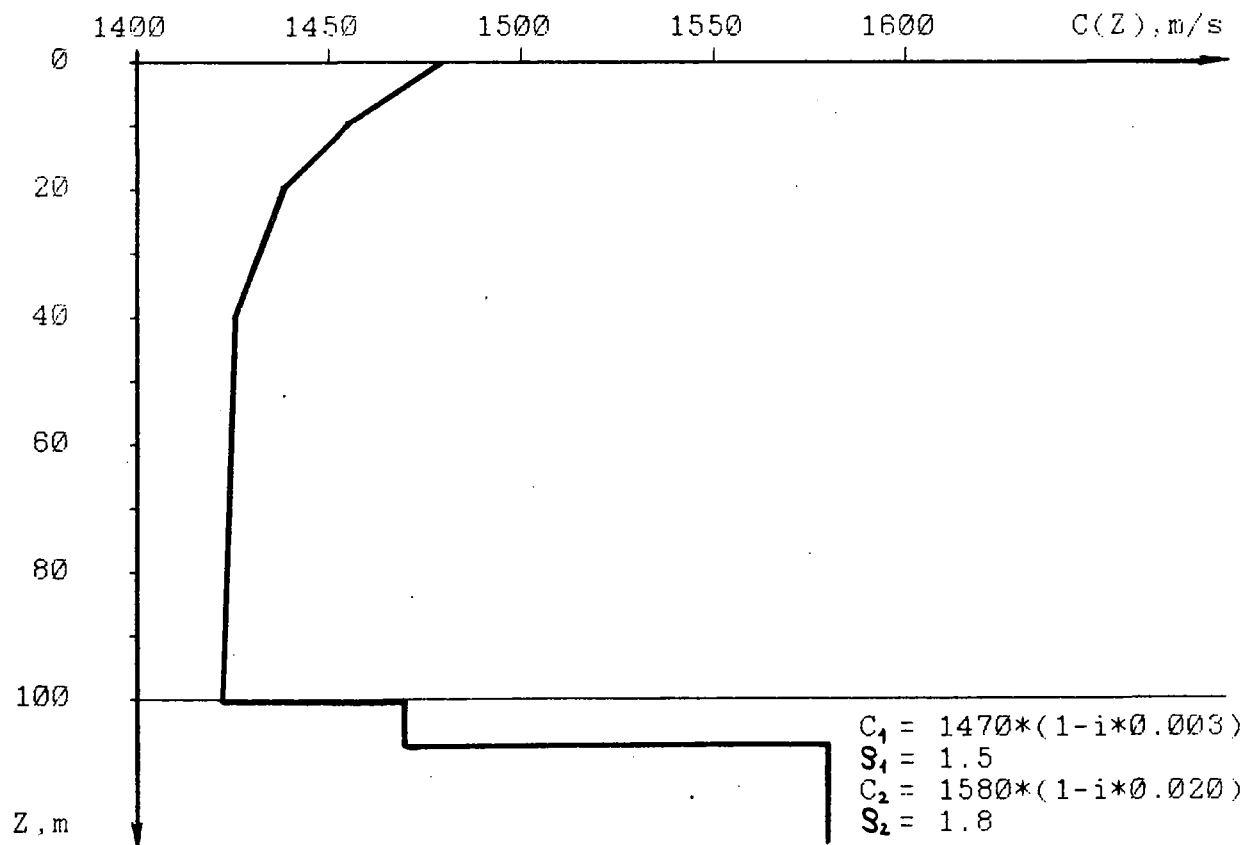
Fig. 3.2 "Summer" waveguide model.

43
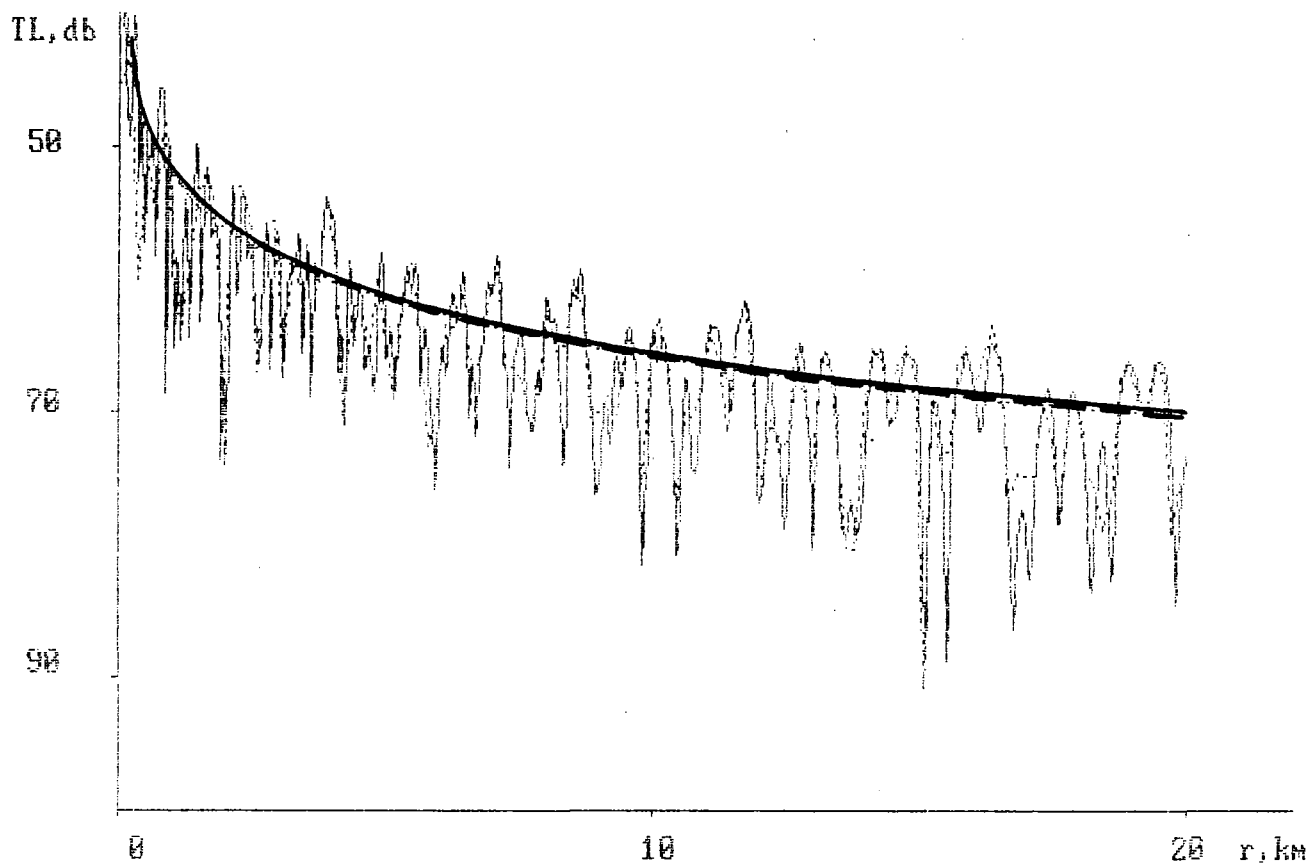
Fig. 3.3   Transmission loss as a function of range
for "winter" waveguide model.

F = 200 Hz , Zo = 75 m , Z = 50 m .

——————————— PE
━━━━━━━━━━ ray invariant
– – – – – – normal mode (coherent)
▬ ▬ ▬ ▬ ▬ ▬ normal mode (incoherent)
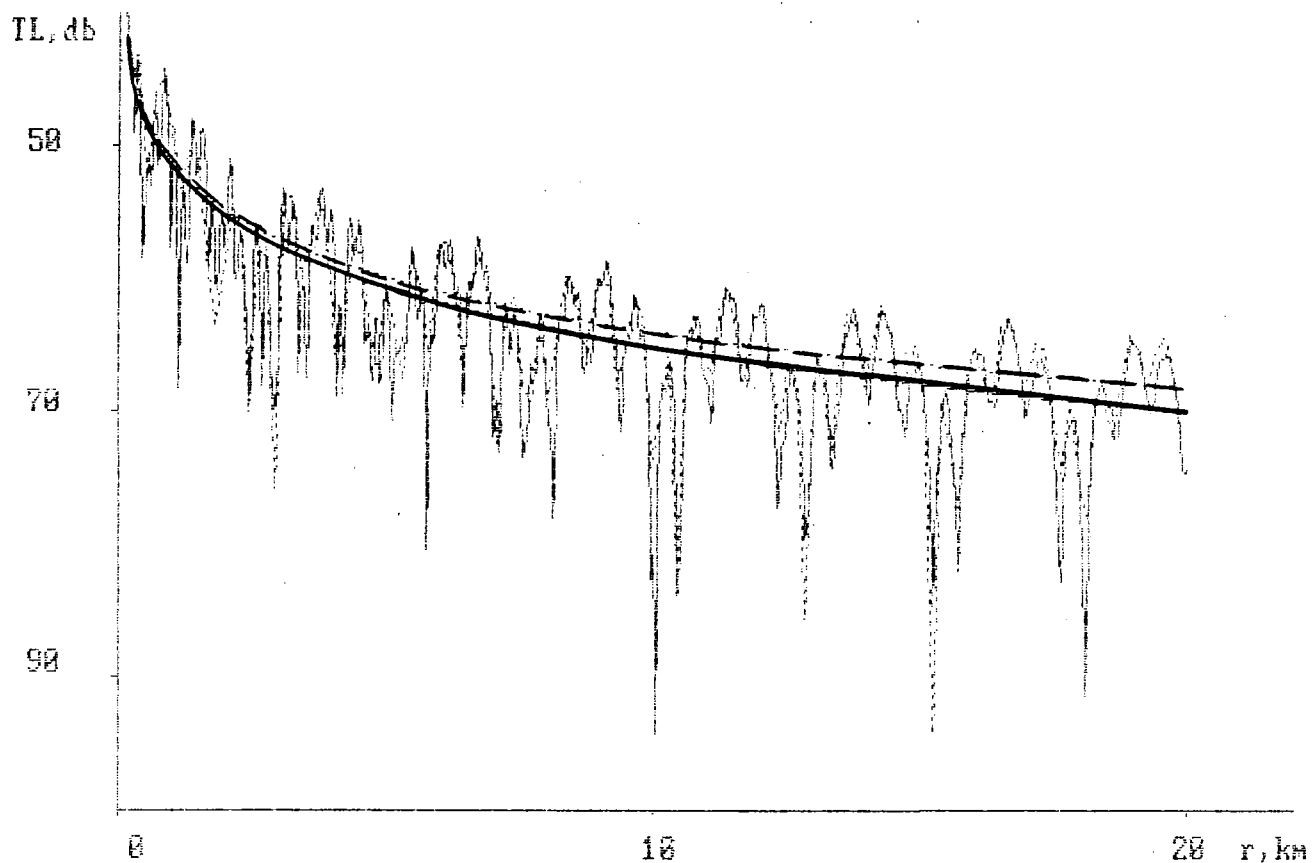
Fig. 3.4   Transmission loss as a function of range
for "summer" waveguide model.

F = 200 Hz , Zo = 75 m , Z = 50 m .

———————————— PE
━━━━━━━━━━━━ ray invariant
— — — — — — normal mode (coherent)
— — — — — — normal mode (incoherent)

this model gives the field averaged over r. As it might be seen from the Fig.3.3, 3.4, in the first case the method of adiabatic invariant describes the integral field decay rather exactly, but in the second one gives the lowered value. Obviously, the precision of ray method depends both on the frequency f and on the depths of source and receiver.

At Fig.3.5 - 3.8 the dependencies of average field level on the depth of receiver z are depicted for two frequencies. It is seen that the ray method of adiabatic invariant is applicable except the cases when $z \rightarrow z_0$ (the divergence region of (3.17)), when the ray approach fails. Also it might be seen, that in the "winter" waveguide the sound field almost does not depend on the depth, except the small region near the surface of about wavelength thickness. As it follows from the boundary conditions the sound field at the surface is exactly equal to 0 . For the summer conditions, owing to the formation of deep sound channel the field level is low within the region of higher sound speeds.

As it follows from mentioned above, the change of the frequency changes the scale of interference field structure both at z and r axes. Moreover, the time variability of hydrological conditions leads to the strong fluctuations of field generated by a harmonic source. Due to that it seems to be expediently to use the averaging of quazimonochromatic noises over time. And because the averaging over frequency is equivalent to the averaging over space, the adiabatic invariant method gives, in fact, the field averaged over time.
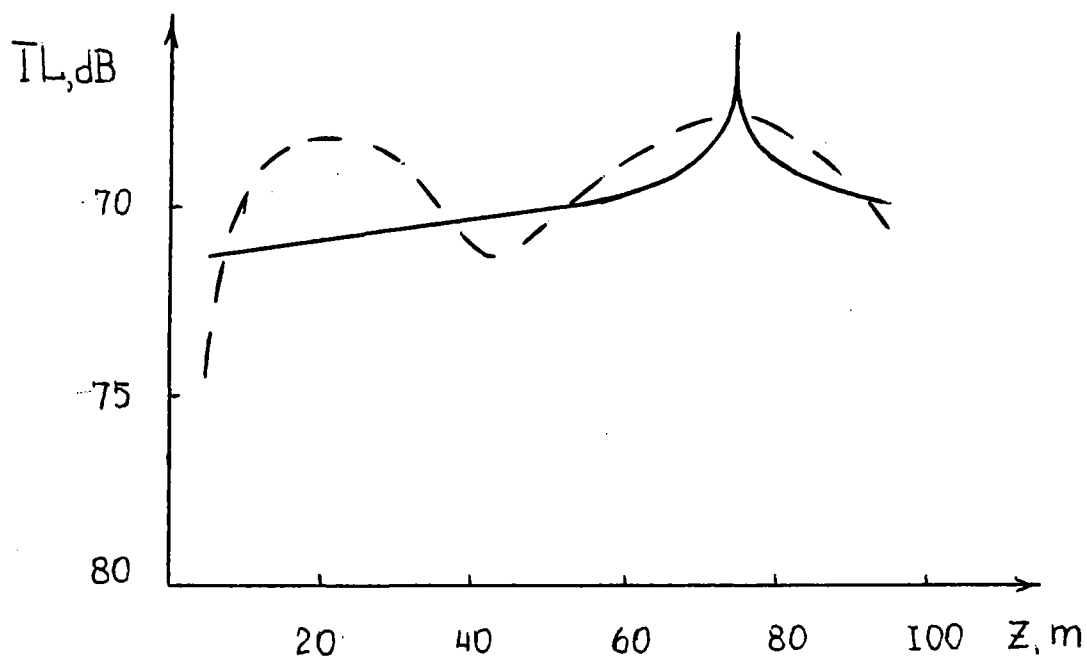
Fig. 3.5   Transmission loss as a function of depth
           for "winter" waveguide model.

           F = 200 Hz , Zo = 75 m , R = 20 km .

           ————————— ray invariant
           — — — — — normal mode (incoherent)

Fig. 3.6   Transmission loss as a function of depth
           for "summer" waveguide model.

           F = 200 Hz , Zo = 75 m , R = 20 km .

           ————————— ray invariant
           — — — — — normal mode (incoherent)
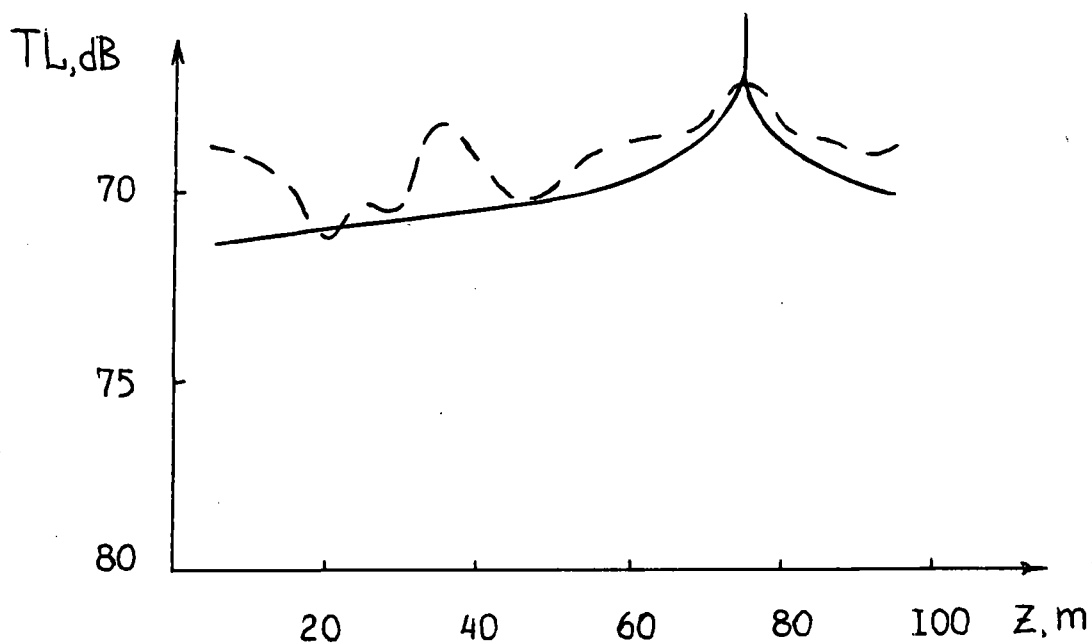
Fig. 3.7   Transmission loss as a function of depth
            for "winter" waveguide model.

            F = 500 Hz , Zo = 75 m , R = 20 km .

            ——————————— ray invariant
            — — — — — — normal mode (incoherent)
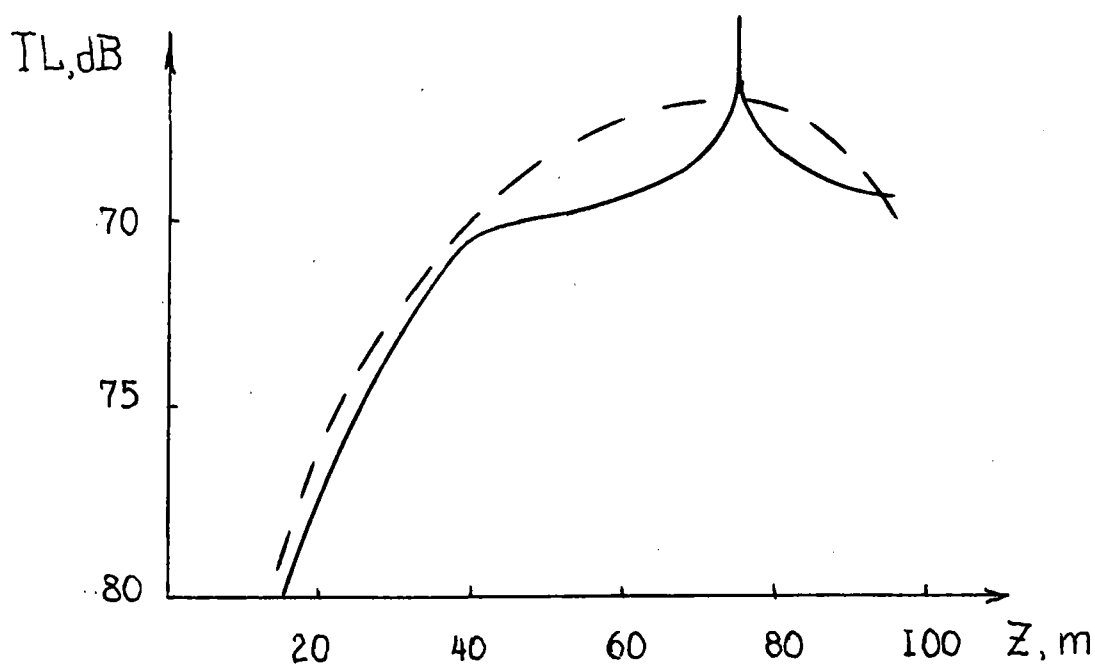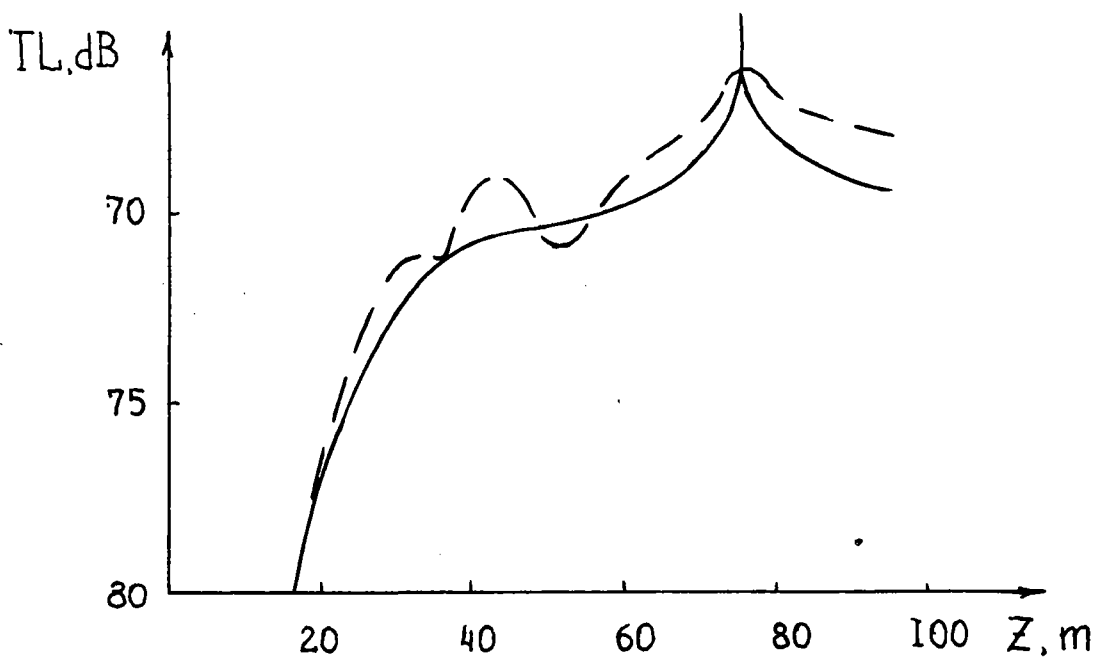

Fig. 3.8   Transmission loss as a function of depth
            for "summer" waveguide model.

            F = 500 Hz , Zo = 75 m , R = 20 km .

            ——————————— ray invariant
            — — — — — — normal mode (incoherent)

48

3.3 TRANSMISSION LOSS IN LAKE ONTARIO ON THE PATH BETWEEN THE WESTERN TIP OF TORONTO ISLAND AND THE MOUTH OF WELLAND CANAL

Here the following problems are considered :
- the estimation of the applicability of the adiabatic invariant method for the range-dependent waveguide with respect to Lake Ontario ;
- the estimation of the field intensity distribution along the chosen path and the analysis of the field structure at different depths for different frequencies.

This chapter might be split into two parts. The first one contains the analysis of the results for typical winter conditions, and the second – for typical summer ones. Sound speed profiles for both seasons and the acoustic model of bottom are presented at figures 3.1.and 3.2. The depth variability (the bottom relief) along the path is shown at Fig.2.2. The thickness and acoustic properties of sediment layers and are supposed to be range – independent.

Winter Hydrology

At figures 3.9 and 3.10 one can see the comparison of range dependencies of transmission loss computed by using the high-angle parabolic equation and the method of adiabatic invariant respectively for the frequencies 100 Hz and 500 Hz. As it could be predicted the precision of the adiabatic invariant method grows up with the increase of signal frequency. But the fact that the field levels in the end of the waveguide at the local maximum calculated by these two different methods are almost equal is the rather surprising one. Because in this section of the waveguide there is only one propagating mode and the adiabatic invariant methods is formally inapplicable!

Let us consider the field changes along the path more detailed. At the first two kilometres there is a rapid field decrease induced by cylindrical divergence and strong

49
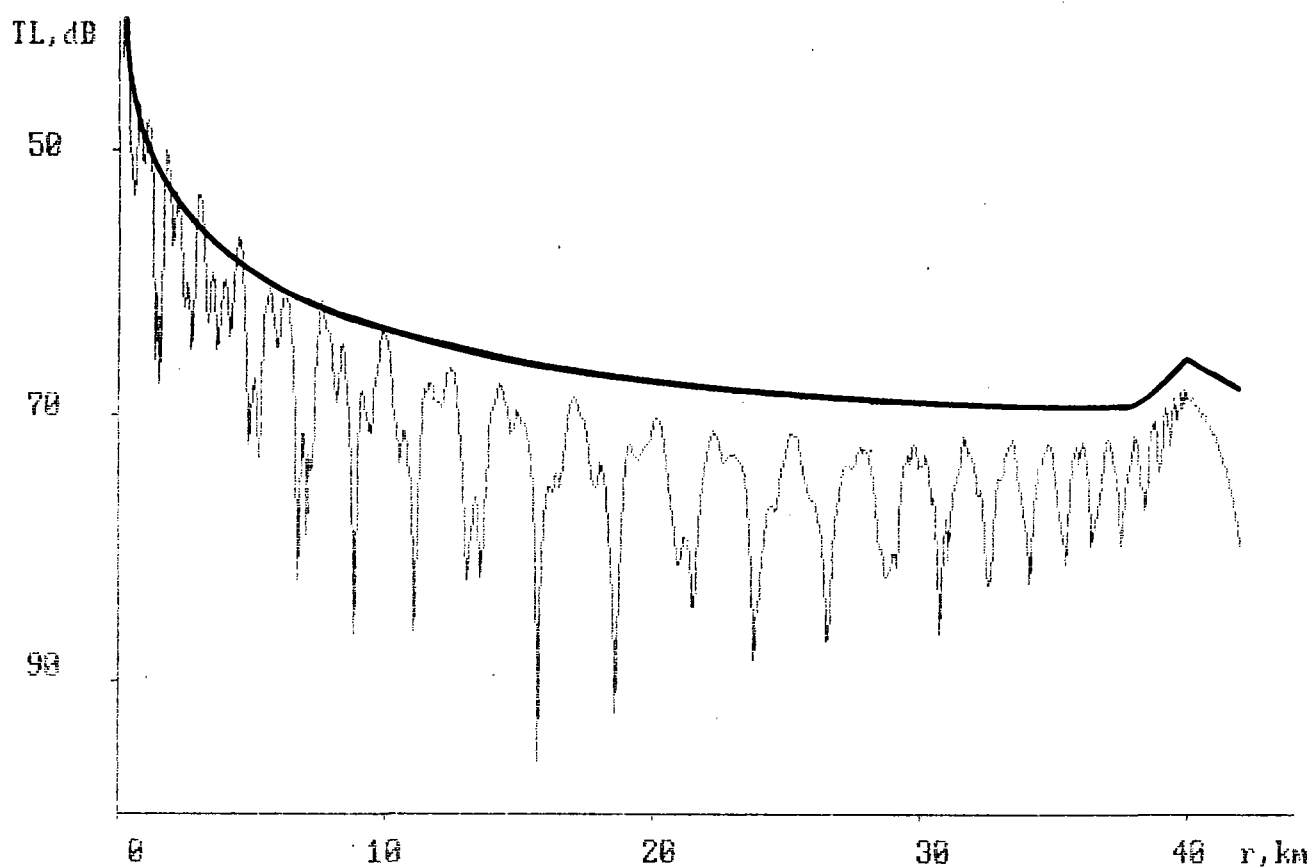
Fig. 3.9   Transmission loss as a function of range
           for "winter" condition.

F = 100 Hz , Zo = 30 m , Z = 10 m .

───────────── PE
━━━━━━━━━━━━━ ray invariant
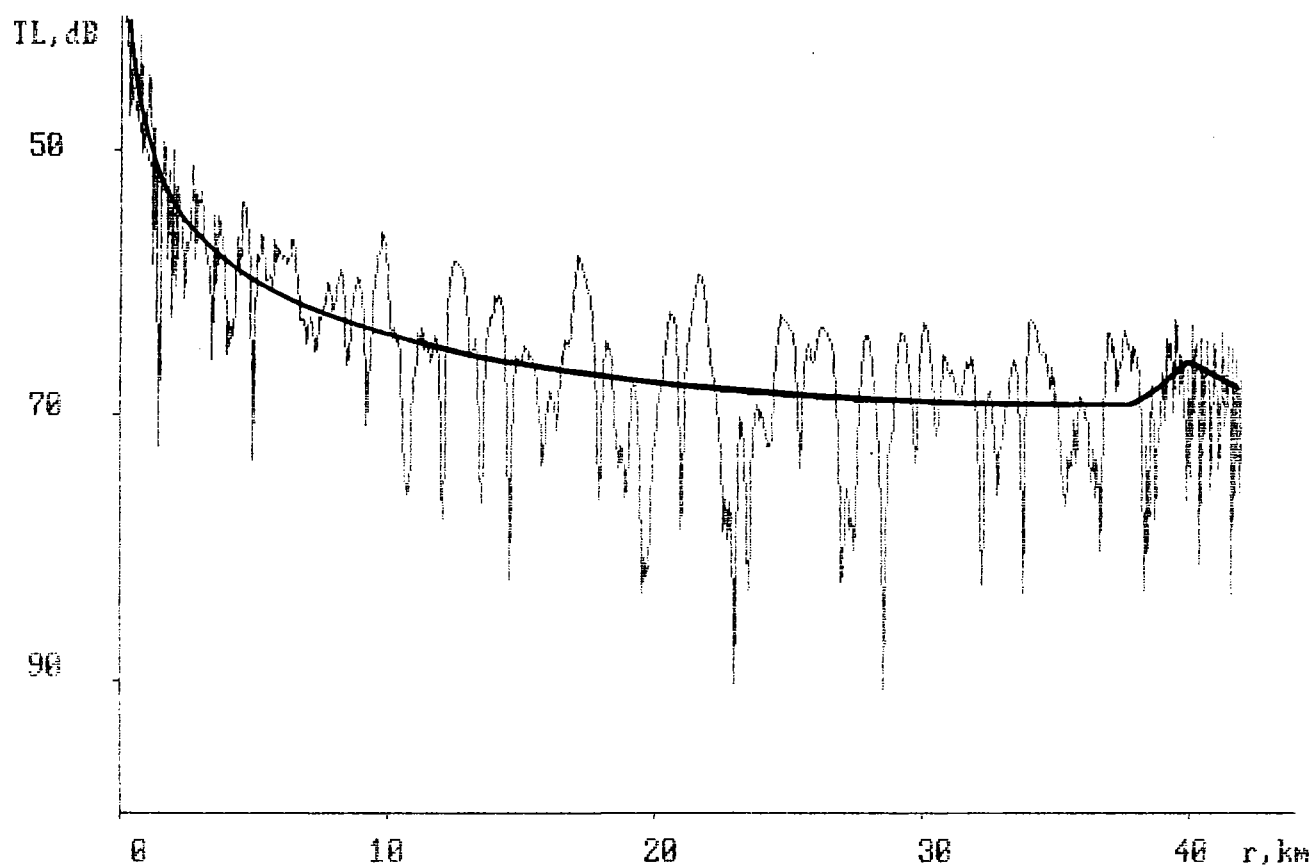
Fig. 3.10 Transmission loss as a function of range
for "winter" condition.

F = 500 Hz , Zo = 30 m , Z = 10 m .

——————————— PE
━━━━━━━━━━━ ray invariant

attenuation of the rays with angles $\chi > \chi_*$ in the bottom. At the main part of the path the field decreases rather slowly. Then with the decrease of waveguide depth, the field intensity increases. But, rays of great inclination cannot reach the narrow waveguide cross-sections, since the grazing angle increases with each reflection from the rising bottom and eventually, the rays are reflected back. As far as normal waves are concerned it means that the propagating mode becomes the nonpropagating one.

The computations of transmission loss in the winter waveguide have been carried out for the frequency band from 100 Hz to 10.000 Hz for the depth range from 10 m to 40 m. The results of these computations shown at Fig.3.11 (shaded area) mean that the changes of f and z do not affect the transmission loss. Such a weak dependence of the transmission loss on the frequency and depth might be explained by the fact that the main contribution into the field energy is made by rays with the small inclination at the bottom. As it follows from Fig.2.6., the reflection coefficient does not almost depend on the frequency.

Thus, the winter conditions seems to be favorable to the acoustic wave propagation. The typical values of transmission loss is limited by 65 dB and weakly depend on the source frequency and the receiver depth.

Summer Hydrology

In summer the conditions of propagation considerably change : the subsurface water layer is heated on and, as a result, the sound speed greatly decreases in the layer about 50 m thick. In the medium with such a hydrology rays bend to the bottom (Fig.1.7.(b)) and reach the bottom at steeper angles, so they are attenuated more strongly than in a plane layered waveguide. The second reason is that if the source is located below the level of receiver, then not all the rays reach the receiver. Obviously, that such hydrology "wrings out" the field from the surface and, as the result, the field level increases with the increase of waveguide depth.
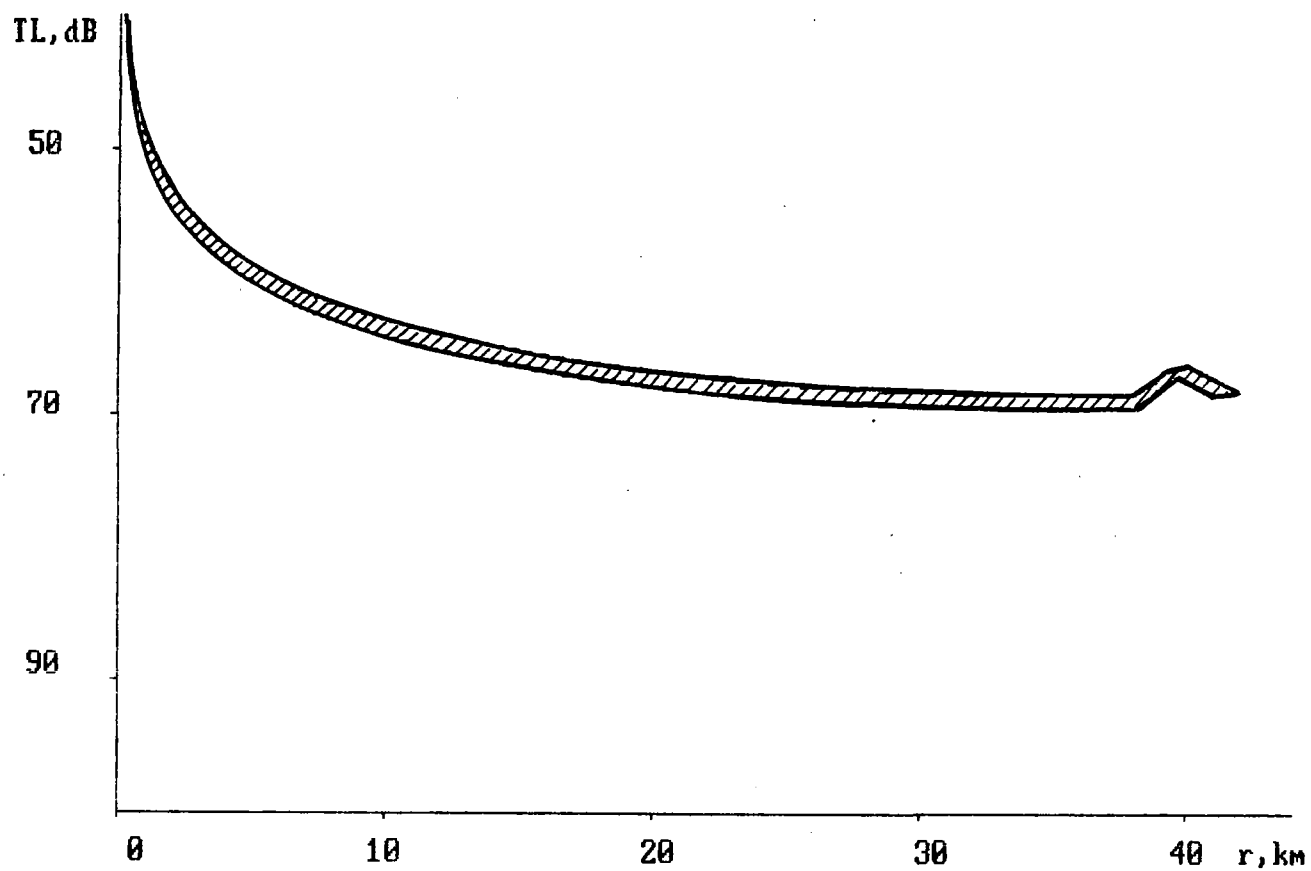
Fig. 3.11   The variability TL for "winter" conditions.

Zo = 30 m ,
Z   = 10 - 40 m ,
F   = 100 - 10000 Hz .

In order to check out the efficiency of the adiabatic invariant method in the medium with the range-dependent hydrology the comparison with the high-angle PE method was made.(Fig.3.12, 3.13). As it is seen from the figures the adiabatic invariant method satisfactory describes the averaged field distribution at the frequencies $f > 500$ Hz.

At Fig.3.14 the range dependencies of transmission loss for different horizons of the receiver are shown. One can see that the field strongly decreases at the small depths of receiver in the medium part of the path, where the waveguide depth is great. However, when the depth of the waveguide is small, the difference between field levels at different receiver horizons becomes less. It is connected with the fact that at long distances the field in the narrow part of the waveguide is determined by the rays of relatively small inclination at the bottom. It might be clearly seen from the Fig.3.15, where the frequency dependencies of the transmission loss at $r = 38$ km for different horizons at the sole of the main slope is depicted. For the depths $z > 15$ m no frequency dependence is visible, since the field formation is determined by the rays of small inclination at the bottom $\chi < 13^\circ$. For these angles the reflection coefficient does not depend on the frequency. In the surface vicinity $z < 15$ m the field is determined by the rays, the inclination of which at the bottom is above this critical value. For the low frequencies the critical angle is determined by the lower half-space and is equal to $\chi_* = 23^\circ$. With the increase of the frequency the critical angle χ_* decreases and becomes equal to 13°. It leads to the appearance of the strong frequency dependence of the transmission loss at small receiver depth in the intermediate frequency region from 200 Hz to 600 Hz.

The data concerning the frequency dependence of the transmission loss are shown at Fig.3.16. It was assumed that the receiver is located at the bottom. The point $L = 0$ corresponds to the horizon $z = 10$ m in the end of the path shown at Fig.2.2. The increase of L corresponds to the shift of the receiver in the direction of the source. It follows from the consideration of these graphics that there exists some optimal distance where the signal level is maximal, which

54
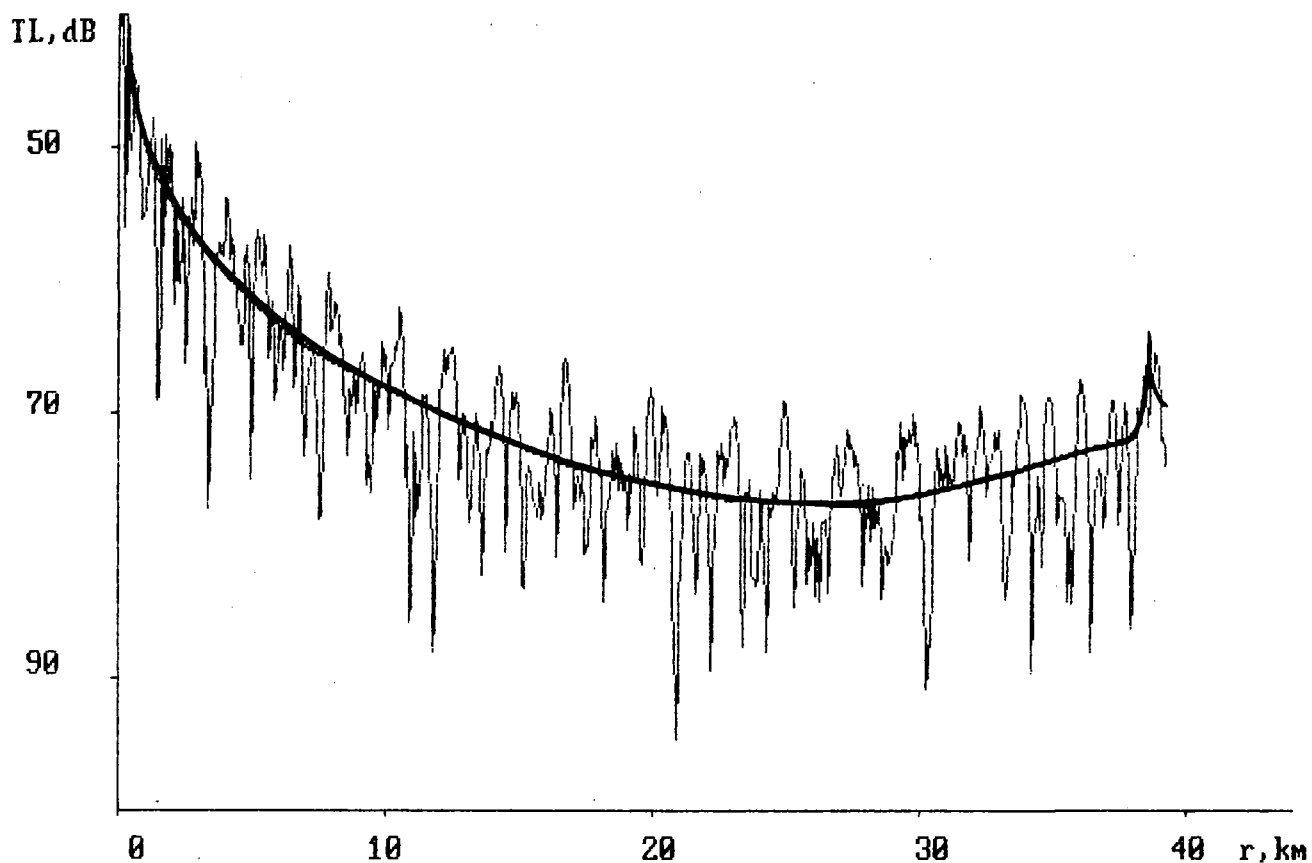
Fig. 3.12   Transmission loss as a function of range
for "summer" condition.

F = 500 Hz , Zo = 30 m , Z = 35 m .

———————————— PE
———————————— ray invariant
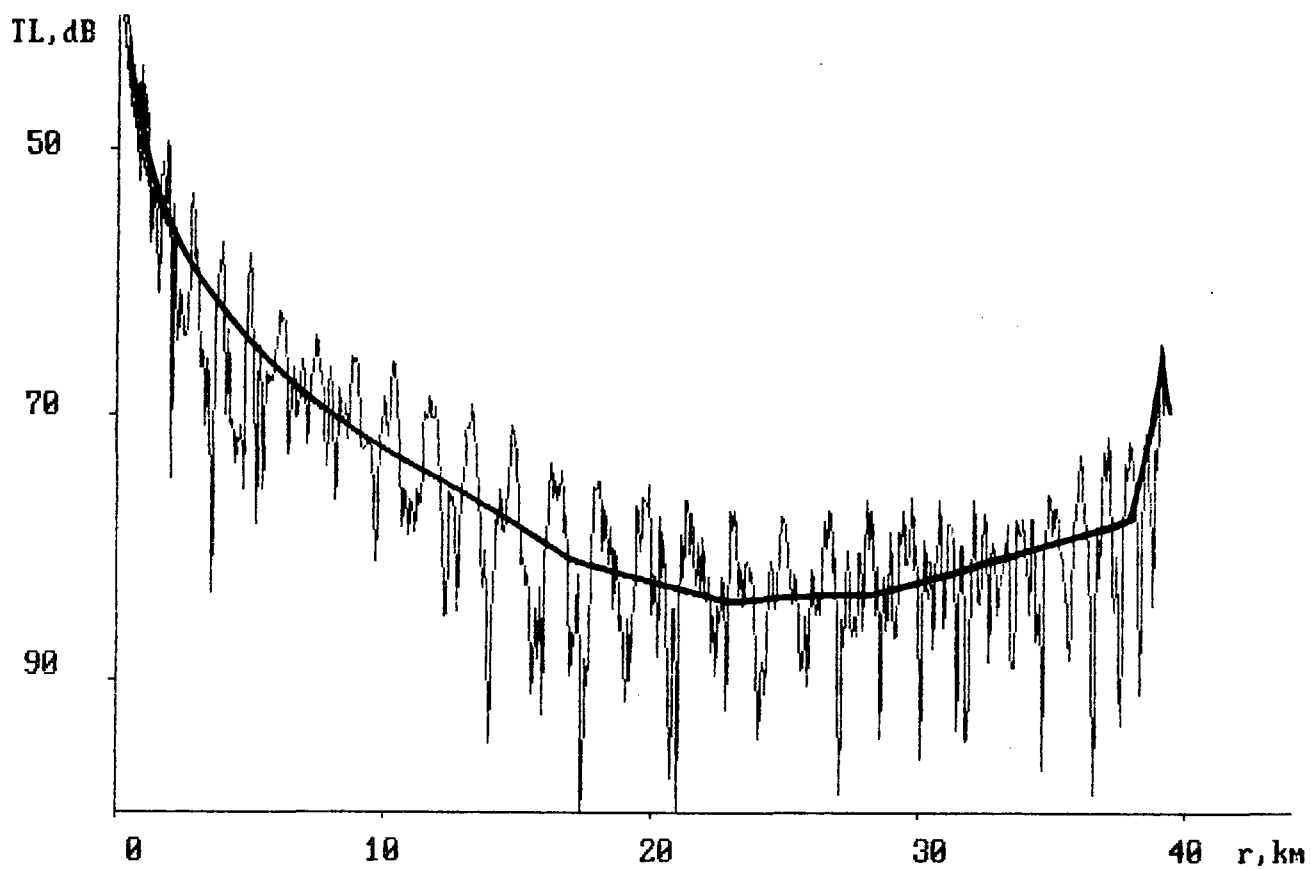
Fig. 3.13   Transmission loss as a function of range
for "summer" condition.

F = 500 Hz , Zo = 30 m , Z = 25 m .

——————————— PE
——————————— ray invariant
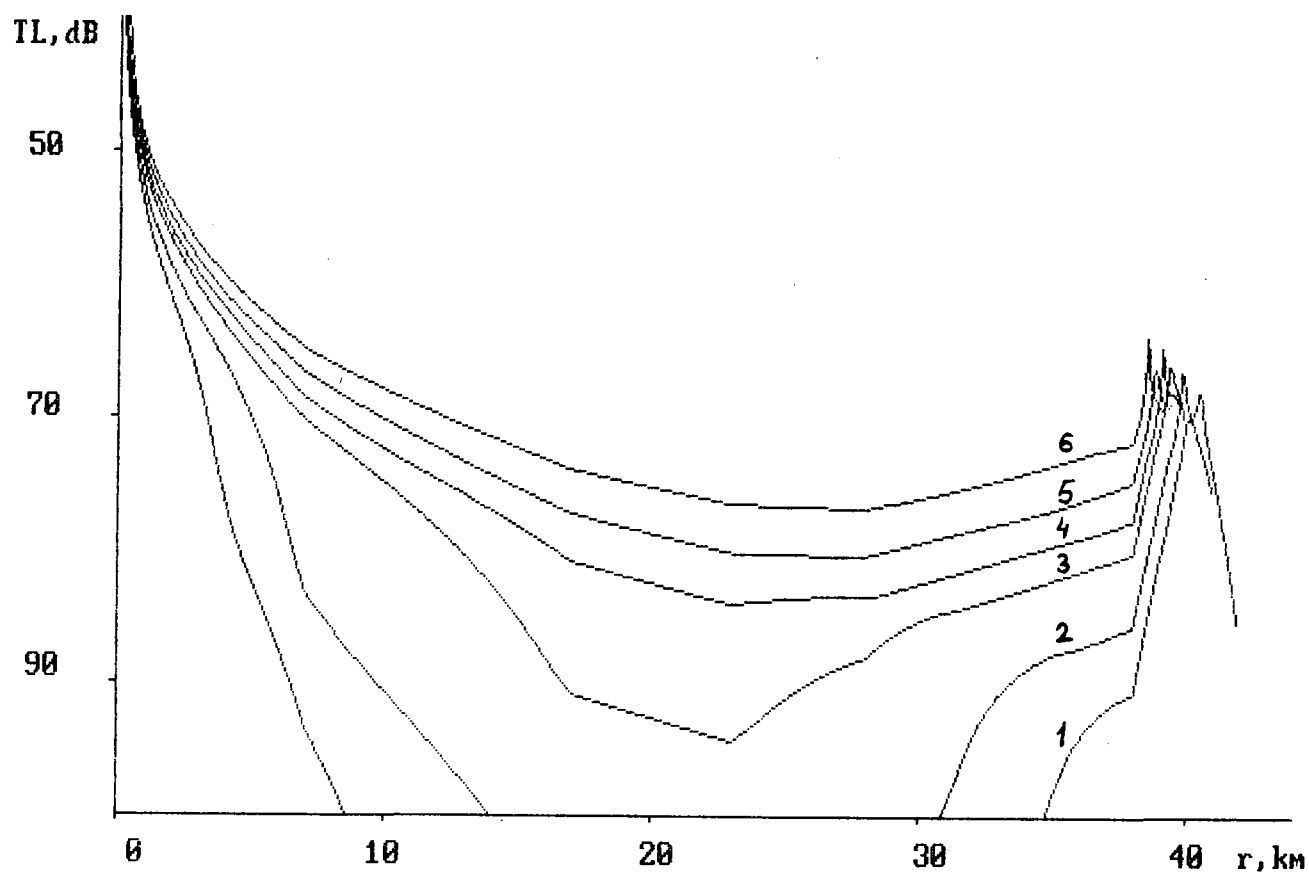
Fig. 3.14   Transmission loss as a function of range
for different depth in "summer" waveguide
model.

F = 500 Hz , Zo = 30 m ,

1 -   Z = 10 m ,
2 -   Z = 15 m ,
3 -   Z = 20 m ,
4 -   Z = 25 m ,
5 -   Z = 30 m ,
6 -   Z = 35 m .
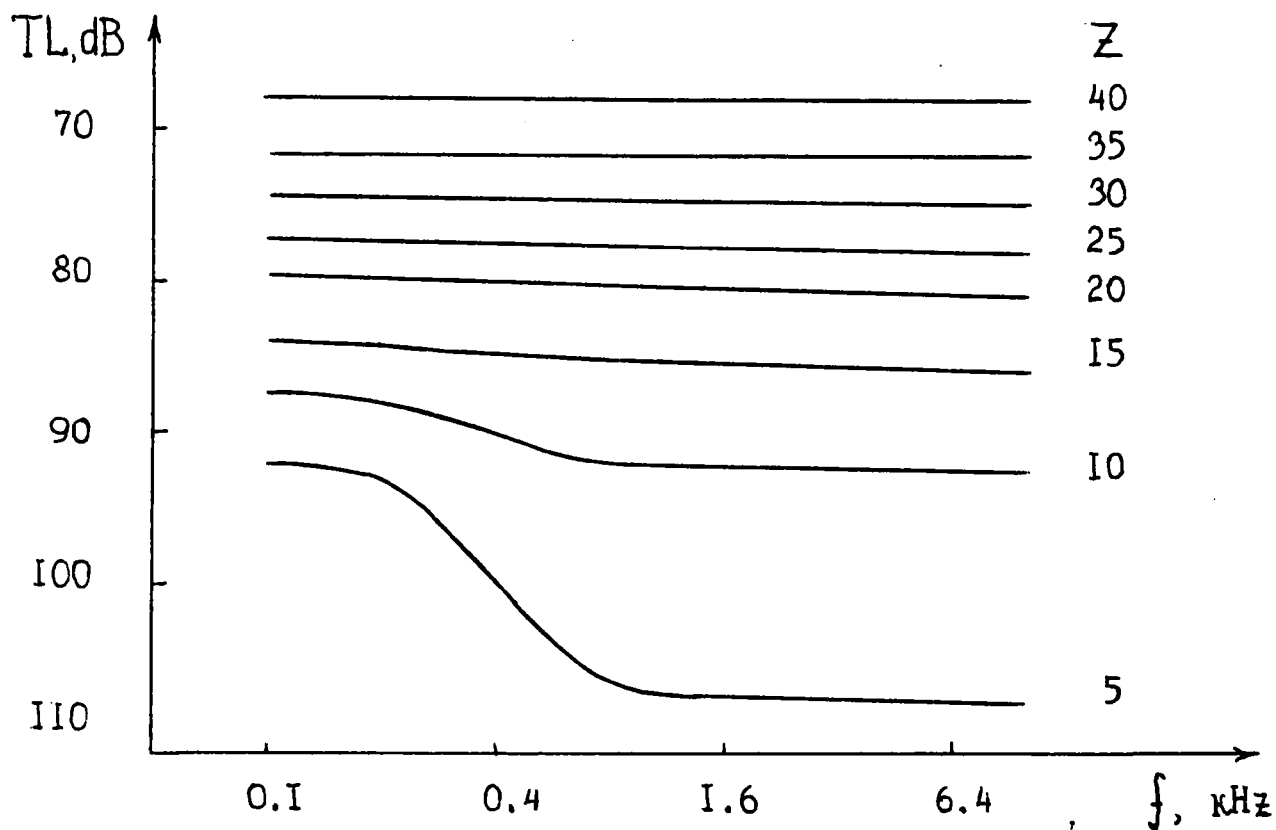
Fig. 3.15 Transmission loss as a function of frequency for different receiver depth in "summer" waveguide model.

Zo = 30 m , R = 38 km .

Fig. 3.16   I - f=100 Hz,
                 2 - f=500 Hz,
                 3 - f=10 kHz.

corresponds to the depth of receiver $z \approx 30 - 40$ m. But since the purpose of the work is 1the diagnostics of bubbles in the subsurface layer, the question of the optimal location of the receiver is still open for the discussion. The problem is that we should find the location of best sensitivity to the subsurface bubble layer and this location might happen is not within the area of maximal intensity of signal.

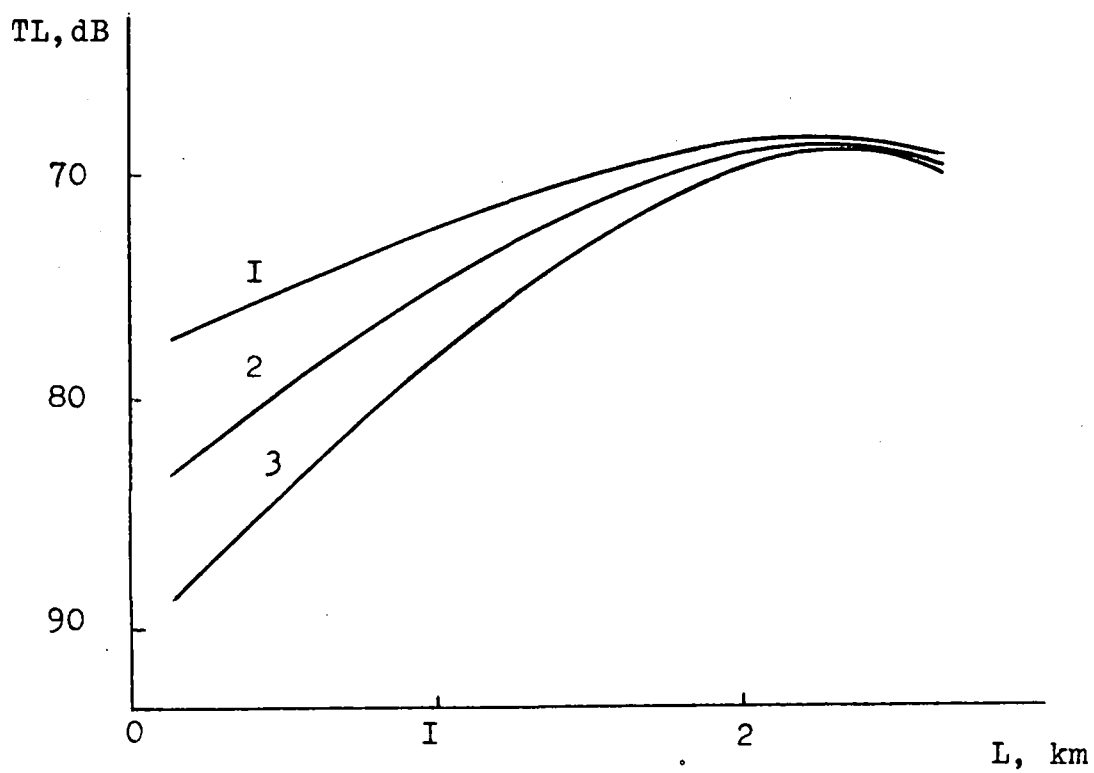In conclusion it is worth noting that summer hydrology is sensitive to even small changes of bottom parameters. Thus, the adding of the thin water-satiated layer with parametres described in Chapter 2.2 to the bottom model leads to the abrupt decrease of the signal level with the increase of the frequency. The variability of transmission loss is rather small for two-layered bottom (Fig.3.17, region 0), but for the model with such a thin layer the transmission loss lies in this region only for the lower frequencies ($f \approx 100$ Hz). For the frequencies $f > 2$ kHz the signal level decreases very quickly. The winter hydrology with the weaker frequency dependence of transmission loss is more convenient for the conduction of experiments on the site (Fig. 3.18).

Hence, in the natural conditions of chose path the signal level (at high frequencies $f > 1$ kHz) is sensitive to the presence of even thin water- satiated layers. That is why the detailed analysis of bottom properties from the acoustic point of view is necessary. The main problem is connected with the estimation of the absorption coefficient in Lake's sediments.

Naturally, the choosing of source power level depends not only on the losses in a bubble layer, but also on the method of received signal processing. Here we estimate approximately the required power level, supposing the bubble induced attenuation to be about 40 dB (see [26]). The calculations are made for the narrow-band ($\Delta f = 1$ Hz) and wide-band ($\Delta f = 100$ Hz) signals of frequency $f = 1$ kHz. As it follows from Fig.3.18, the maximal noise level is about 40 dB. The typical value of transmission loss for such conditions is 70 dB, i.e. for the narrow-band signal one needs the source power level to be about 150 dB (it corresponds to the acoustic power 10^{-2} W) and for the wide-band signal – about 170 dB (acoustic power 1 W).

Fig. 3.17   Transmission loss as a function of
range at different frequencies in
"summer" waveguide for two models
of bottom.:
0 - no water - satiated layer,
I,2,3,4 - with the thin water - satiated
layer.

I - f = I00 Hz ,
2 - f = I kHz ,
3 - f = 2 kHz ,
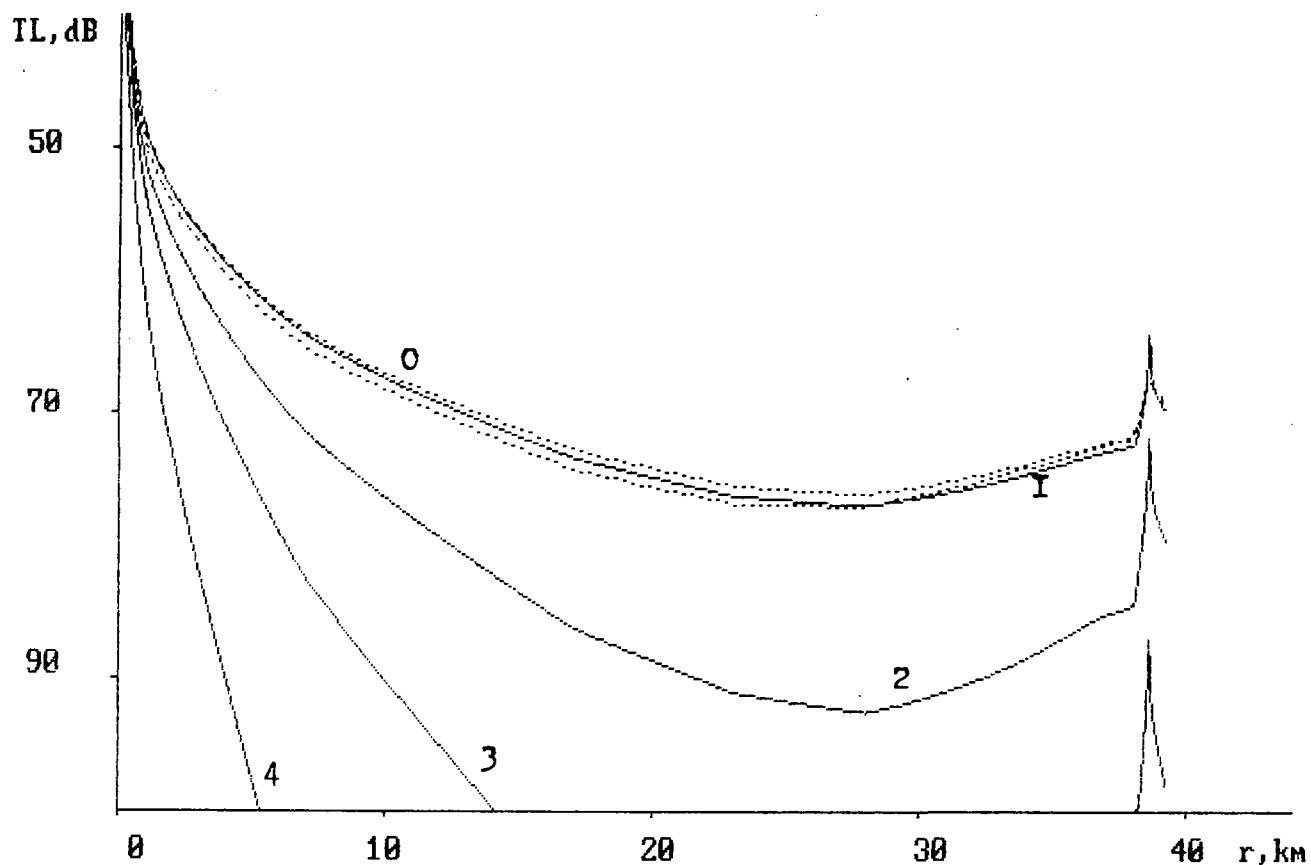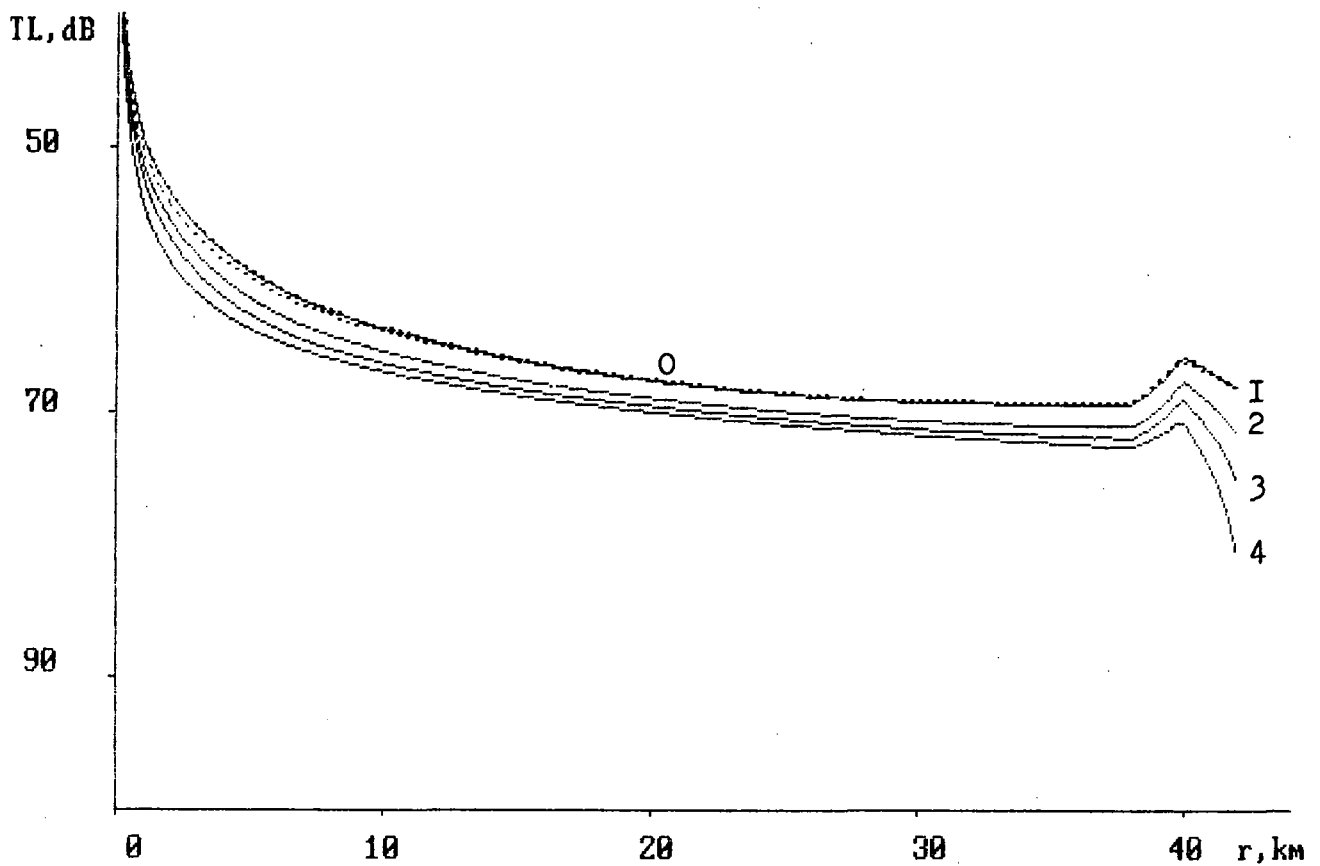4 - f = 5 kHz .

$Z_0 = 30$ m , $Z = 35$ m.

Fig. 3.18   Transmission loss as a function of
range at different frequencies   in
"winter" waveguide for two   models
of bottom :
0 - no water - satiated layer ,
I,2,3,4 - with the thin water - satiated
              layer.

I - f = I00 Hz ,
2 - f = I kHz ,
3 - f = 2 kHz ,
4 - f = 5 kHz .

Z_0 = 30 m , Z = I0 m.

Appendix A.

CALCULATION OF AVERAGE SOUND FIELD INTENSITY IN RANGE – DEPENDENT WAVEGUIDES USING ADIABATIC INVARIANT METHOD

General formulation

In [29] the expressions for average intensity of sound field in plane layered waveguide are introduced within the framework of ray approach. The generalization of this approach for the range – dependent ducts might be found in [30]. There the agreement of the results obtained from ray and wave theories is discussed as well. Below we follow these two works in general, though some details might be slightly different.

Let us consider the cylindrically symmetric waveguide with the sound speed profile $c = c(z,r)$. The sound field generated in such waveguide by point harmonic source in the adiabatic approach of normal waves method is given by [29] :

$$p(z,r)=(2\pi/r)^{1/2} \sum_n \frac{\psi_n(z_o,0)\psi_n(z,r)}{(\xi_n(r))^{1/2}} \, exp\left[i\int_0^r \xi_n(r)dr - \frac{i\pi}{4}\right], \text{(A1)}$$

where $(z_o,0)$ – the coordinates of source,

(z, r) – the coordinates of receiver,

$\xi_n(r)$ – the eigenvalues,

$\psi_n(z,r)$ – the eigenfunctions.

The intensity of sound field, averaged over range r in this case is described as follows :

$$\langle I \rangle = \langle pp^* \rangle = \frac{2\pi}{r} \sum_n \frac{|\psi_n(z_o,0)|^2|\psi_n(z,r)|^2}{Re \, \xi_n(r)} \, exp\left[-2\int_0^r Im \, \xi_n(r)dr\right]. \text{(A2)}$$

If the number of propagating modes is great and the depth dependence of wave number $k(z,r) = \omega/c(z,r)$ at any fixed range

r has the only one maximum, then to find out the eigenfunctions one can use the WKB approximation [50]:

$$\phi_n(z,r) = 2 \left[\frac{Re_n \xi(r)}{\ae_n(z,r)D_n(r)} \right]^{1/2} \cos \left\{ \int\limits_{z_n' \text{ or } z_n''}^{z} \ae_n(z,r)dz + \phi_n(r) \right\}, \quad (A3)$$

$$D_n(r) = 2 \, Re \, \xi_n(r) \int\limits_{z_n'}^{z_n''} \frac{dz}{\ae_n(z,r)} , \quad (A4)$$

$$\ae_n(z,r) = \left[(\, k^2(z,r) - (\, Re \, \xi_n(r) \,)^2 \right]^{1/2}, \quad (A5)$$

where $z_n'(r)$ and $z_n''(r)$ – the depths, within which the normal wave is concentrated,

$| \, \phi_n(r) \, | < \pi$ – the additional phase, depending on the kind of normal wave.

Substituting (A3) into Eq.(A2) and averaging over depths z and z_0 we obtain

$$\langle I \rangle = \frac{8\pi}{r} \sum_n \frac{Re \, \xi_n(r)}{\ae_n(z_0,0)\ae_n(z,r)D_n(0)D_n(r)} \, exp \left[-2\int\limits_0^r Im \, \xi_n(r)dr \right]. \quad (A6)$$

The real part of eigenvalues might be found from the expression for the phase integral in WKB approximation :

$$J(r) = \int\limits_{z_n'}^{z_n''} \ae_n(z,r)dz = \int\limits_{z_n'}^{z_n''} \left\{ (k^2(z,r) - (Re \, \xi_n(r))^2 \right\}^{1/2} dz = n\pi + \vartheta_n(r), \quad (A7)$$

where $| \, \vartheta_n(r) \, | < \pi$ – the additional phase, depending on the kind of normal wave.

64

Within the WKB approximation each normal wave might be considered as the system of rays :

$$Re \; \xi_n(r) = k(z,r) \; cos \; \chi(z,r) \; . \tag{A8}$$

If the parameters of waveguide slowly varies within the ray cycle, i.e. each cycle does not strongly differs from the previous one, then for the particular ray one can suppose J to constant. (In fact, it is the condition of adiabaticity and J/ω is an ray adiabatic invariant). The assumption made allows to obtain two important conclusions. At first, using J one can link the departure angle of ray χ_o with its angle at the horizon of receiver χ. Second, in Eq.(A6) one can change the summation over n to the integration over angle χ_o (or χ). Using (A7) and taking into account (A3)-(A5) and (A8) the following expression might be obtained :

$$dn = \frac{dJ}{\pi} = \frac{\ae(\chi_o,0) \; D(\chi_o,0)}{2\pi} \; d\chi_o = \frac{\ae(\chi,r) \; D(\chi,r)}{2\pi} \; d\chi \; . \tag{A9}$$

As a result we find :

$$\langle I \rangle = \frac{4}{r} \int_0^{\pi/2} (\; tg \; \chi \quad D(\chi,r) \;)^{-1} \; exp\left[-2\int_0^r \beta(\chi,r)dr\right] d\chi_o \tag{A10}$$

or

$$\langle I \rangle = \frac{4}{r} \int_0^{\pi/2} (\; tg \; \chi_o \; D(\chi_o,0) \;)^{-1} exp\left[-2\int_0^r \beta(\chi,r)dr\right] d\chi \; . \tag{A11}$$

Here $\quad \beta(\chi,r) = \dfrac{ln \; | \; V(\chi',r \;)|}{D(\chi,r)} \tag{A12}$

is the loss function for bottom interacting rays, $V(\chi',r)$ is the bottom reflection coefficient, and angles χ and χ' are connected by Snell's law :

$$k(z,r) \; cos \; \chi = k(H,r) \; cos \; \chi' \; , \tag{A13}$$

where r is introduced as a parameter.(The generalization of (A12) for the case of bubble layer induced attenuation might be made easily). Thus, the formulae (A10)-(A13) allows to calculate the average sound field intensity in a range - dependent waveguide.

Numerical algorithm

The description of numerical algorithm presented below requires to consider the medium of propagation. The values of sound speed $c(z_{i,j}, r_i)$ at the fixed distances r_i supposed to be given on the upper ($z=0$) and lower ($z=H(r_i)$) boundaries and at some depths $z_{i,j}$ between (see Fig. A.1). To make the following computation more convenient the waveguide is divided into the space segments, using the linear interpolation both of wave number square $k^2(z,r)$ and of lower waveguide boundary $H(r)$ as it is shown at Fig.A.2. A segment is triangle-shaped, if one of its boundaries is the inclined bottom, and is of rectangle shape otherwise. In segments of the first kind the wave number approximation is $k^2(z,r) = a_0 + a_1 z + a_2 r$, the wave number in the second kind of segments is approximated as $k^2(z,r) = a_0 + a_1 z + a_2 r + a_3 zr$. Thus, for a fixed range r the depth dependence of wave number square is line - broken, so it allows to use the implicit expressions for computation of the integrals (A4) and (A7).

The bottom is represented as a structure which consists of some liquid layers upon the liquid or solid half-space. The reflection coefficient of such bottom is calculated using the recurrent relations [28].

Taking into account all the above one can calculate the transmission loss using adiabatic approach in accordance to the following algorithm.

First, the invariant values $J(\chi_{o,l}, 0)$, the cycle lengths $D(\chi_{o,l}, 0)$ and the loss functions $\beta(\chi'_{o,l}, 0)$ for the rays which leave source at the angles $\chi_{o,l} = \Delta\chi\, l$ are to be calculated. (Here $l = 0,1,...N$, $\Delta\chi = \chi_*/N$, $N + 1$ - is the number of rays)

66

Fig. A.1 grid labels:

c_{00} c_{10} c_{20} c_{30} c_{40} r

c_{01} c_{11} c_{31}

c_{21} c_{41}

c_{02} c_{32}

c_{12} c_{22} c_{42}

c_{03} c_{33} c_{43}

c_{13}

c_{23}

z

Fig. A.I

Fig. A.2 grid labels:

k_{00} k_{10} k_{20} k_{30} k_{40} k_{50} k_{60} r

k_{01} k_{11} k_{21} k_{31} k_{41} k_{51} k_{61}

k_{02} k_{12} k_{22} k_{32} k_{42} k_{52} k_{62}

k_{03} k_{13} k_{23} k_{33} k_{43} k_{53} k_{63}

k_{04} k_{14} k_{24} k_{34} k_{44} k_{54} k_{64}

k_{05} k_{15} k_{25} k_{35} k_{45} k_{55} k_{65}

k_{66}

k_{36}

z
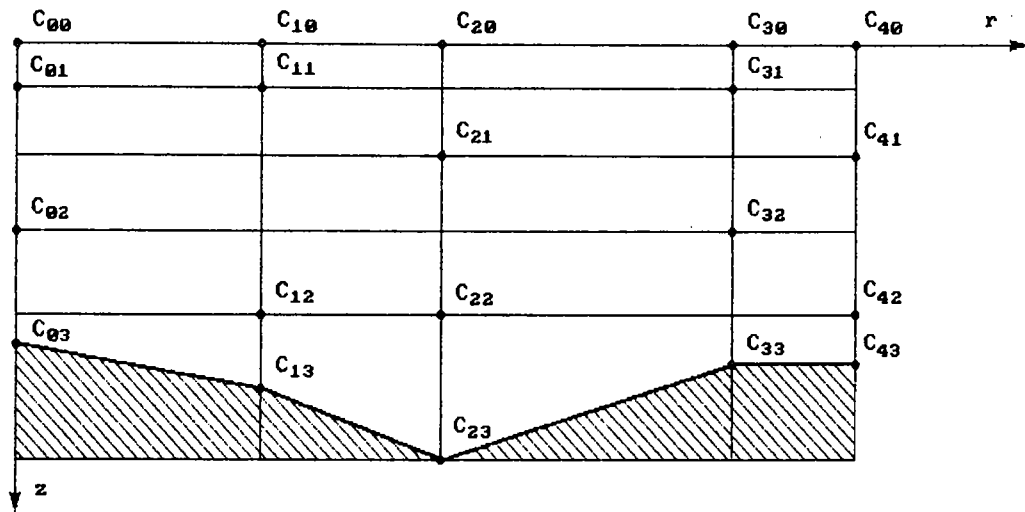
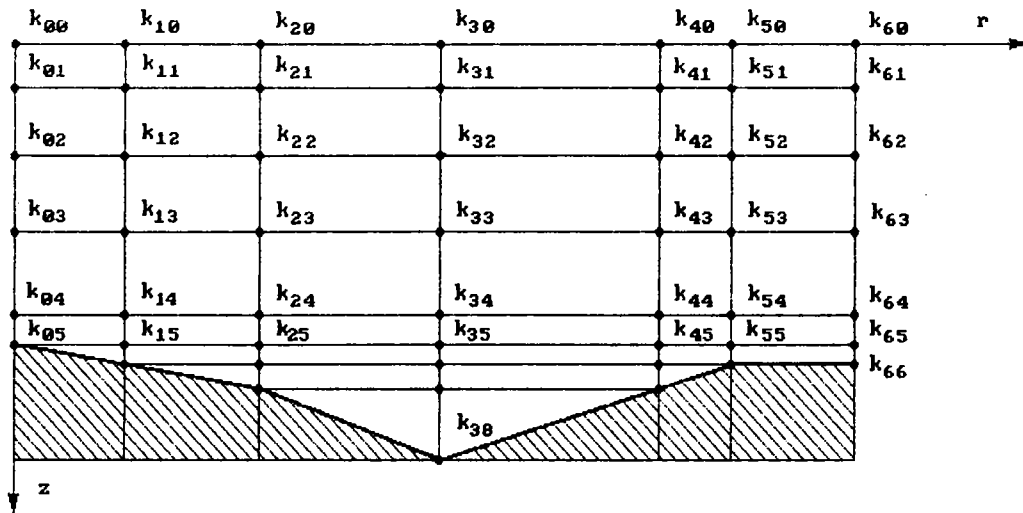Fig. A.2

Then, for the distances $r_k = \Delta r\ K$ ($K = 1,2,\ldots$) the characteristics of rays and the sound field intensity at the receiver horizon are to be calculated. These computations are conducted as follows.

First of all, the invariants $J(\chi_m, r_k)$ of rays of inclination angles at the minimal sound speed horizon $\chi_m = \Delta\chi\ m$ ($m = 0,1,\ldots,M$; $M = int\ (\ \pi\ /\ 2\Delta\chi\ )\ )$ are calculated. If $J(\chi_m, r_k) \leqslant J(\chi_{0,l}, 0) \leqslant J(\chi_{m+1}, r_k)$, $0 \leqslant m \leqslant M-1$, then the ray of departure angle $\chi_{0,l}$ reaches the horizon of the minimal sound speed at the angle χ_l, which might be calculated using the linear interpolation :

$$\chi_l = \chi_m + \Delta\chi\ \frac{J(\chi_{0,l}, 0) - J(\chi_m, r)}{J(\chi_{m+1}, r_k) - J(\chi_m, r_k)}\ , \tag{A14}$$

and for this ray the cycle length $D(\chi_l, r_k)$ and loss function $\beta(\chi_l, r_k)$ are to be computed. The rays for which $J(\chi_{0,l}, 0) \geqslant J(\chi_m, r_k)$ do not reach the range r_k so they are not considered in the following computations. Thus, the characteristics of all the rays which reach the horizon of the minimum sound speed at range r_k are determined. Integral of losses in the expression (A10) is to be computed for each ray using the trapezoid rule:

$$\int\limits_{0}^{r+\Delta r} \beta(r)dr = \int\limits_{0}^{r} \beta(r)dr + \frac{\beta(r) + \beta(r+\Delta r)}{2} \tag{A15}$$

Then from found angles χ_l the angles at the receiver horizon might be calculated using the Snell's law (A13). If the ray of departure angle $\chi_{0,0} = 0$ reaches the receiver, then the integration is made over this departure angles (A10). Otherwise, the integration is to be made over the angles at the receiver horizon (A11). It allows to escape the divergence of integrand. The integration of (A10) or (A11) are made using the trapezoid rule.

REFERENCES

1. Clay C.S., Medwin H. Acoustical oceonography: Principles and applications./ A Wiley-interscience publication. New York - London- Sydney- Toronto, 1977.

2. Devin C. Survey of thermal, radiation and viscous damping of pulsating air bubbles in water. // J.Acoust. Soc.Amer. 1959. V. 31. N 12. P. 1654-1667.

3. Hall M.H. A comprehensive model of wind-generatad bubbles in the ocean and predictions of the effects on sound propagation at frequencies up to 40 kHz. // J.Acoust.Soc.Amer. 1989. V. 86. N 3. P. 1103-1117.

4. Sea surface sound. Natural mechanisms of surface generated noise in the ocean. / Ed. B.Kerman. Kluwer academic publishers. Netherlands. 1988.

5. The physics of sound in the sea. Techn. Report. N.S..Navy. D.C.. 1946.

6. Carstensen E.L.,Foldy L.L. Propagation of sound through, a liquid conteining bubbles.// J.Acoust.Soc.Amer. 1947. V.19. N.3. P.481-501.

7. Gavrilov L. Contents of free gas in liquids and acoustic methods of its measurement. // Sov.Phys. Acoustics. 1969. V.15. N.3.

8. Eller A.I. Damping constants of pulsating bubbles.// J.Acoust.Soc.Amer. 1970. V.47. N.5. P.1469-1470.

9. Medwin H. In situ acoustic measurements of bubble population in coastal ocean waters. //J.Geophys.Research 1970. V.75. N.3. P.599-611.

10. Medwin H. Counting bubbles acoustically.// Review. Ultrasonics. 1977. V.15. N.1, P.7-13.

11. Medwin H. Acoustical determination of bubble-size spectra. // J.Acoust.Soc.Amer. 1977. V.62. N.4. p.1041.

12. Medwin H. In situ acoustic measurements of microbubbles at sea.// J.Geophys.Research. 1977. V.82. P.971-976.

13. Lovik A. Acoustic measurements of gas bubble spectrum in water. In: Cavitation and inhomogeneities in underwater acoustics. /Ed.W.Lauterborn. Berlin-Heidelberg-New York. Springer-Verlag. 1980.

14. Schippers Ir.P. Density of air-bubbles below the sea surface, theory and experiments. In: Cavitation and inhomogeneities in underwater acoustics/Ed W.Lauterborn. Berlin-Heidelberg-New York. Springer- Verlag. 1980.

15. Fenlon F.H. On the amplification of modulated acoustic waves in gas-liquid mixtures. In: Cavitation and inhomo-geneties in underwater acoustics./ Ed. W.Lauterborn . Springer- Verlag. Heidelberg-New York. 1980. P.141-150.

16. Gimenez G., Chamant M., Farnand J.P. Non-linear responce of a single bubble driven by a two-components exciting wave. Proc. 10-th Int.Symp.on Nonlinear Acoustics. Kobe. Japan. 1984. P.83-87.

17. Akulichev V., Bulanov V., Klenin S. Acoustic probing of gas bubbles in the sea.//Sov.Phys.Acoust. 1986. V.32.

18. Thorpe S.A. On the clouds of bubbles formed by breaking wind-waves in deep.waters, and their role in air-sea gas transfer.// Phys. Trans. R.Soc. Lond. 1982. A-304. p.155-210.

19. Urick R.J. Principles of underwater sound. McGraw-Hill Book Company. 1975.

20. Zabolotskaya E., Soluyan S. The radiation of harmonics and combination frequencies by air bubbles.// Sov. Phys. Acoustics. 1972. V.18. N.3.

21. Donskoi D., Zamolin S., Kustov L., Sutin A. Nonlinear backscattering of acoustic waves in a bubble layer. // Acoustics Letters. 1984. v.7. p.134-135.

22. Kobelev Yu., Sutin A. Frequency difference generation in liquids with bubbles of different sizes.// Sov. Phys. Acoust. 1980. V.26. N.6.

23. Gurbatov S.N., Kustov L.M. Acoustic probing of nonstationary emerging bubbles layers.// Sov. Phys. Acoust. 1990. V. 36. N.26. P. 262-268.

24. Ostrovsky L., Sutin A. Nonlinear sound scattering from subsurface bubble layers. In: Natural physical sources of underwater sound./ Ed.B.R.Kerman. Kluwer Academic Publishers. Netherlands. 1993.

25. Sandler B., Selivanovsky D., Sokolov A. Measurement of gas bubble concentration in the subsurface layer of the sea.//Doklady Akademii Nauk SSSR. 1991. V.260. P.1474-1476 (in Russian).

26. Wille P.C., Geyer D. Simulteneous measurements of surface generated noise and attenuation at the fixed acoustic shallow water range. In:Sea surface sound. Natural mechanisms of surface generated noise in the ocean. / Ed. B.Kerman. Kluwer academic publishers. Netherlands. 1988.

27. Jonson B.D., Cooke R.C. Bubble population and spectra in coastal waters: a photographic approach // J.Geophys. Res. 1979. V. 84. P. 3761-3766.

28. Brekhovskikh L.M. Waves in layered media. New York : Academic. 1960.

29. Brekhovskikh L.M., Lysanov Yu.P. Theoretical fundamentals of ocean acoustics. Berlin. Springer. 1982.

30. Smith P.W.Jr. Averaged sound transmission in range-dependent channels. // J.Acoust.Soc.Am. 1974.V.55. P.1197-1204.

31. Medwin H. Speed of sound in water: a simple eqyuation for realistic parameters//J.Acoust.Soc.Amer. 1975. V.58. N.6. P.1318-1319.

32. Hamilton E.L. Geoacoustic modeling of the sea floor// J.Acoust.Soc.Amer. 1980. V.68. N.5. P.1313-1340.

33. Wenz G Acoustic ambient noise in the ocean: spectra and sources// J.Acoust.Soc.Am. 1962. V.34. N 12. P.1936-1956

34. Wille P.C., Geyer D. Measurements of the origin of the wind-dependent ambient noise variability in shallow water. // J.Acoust.Soc.Am. 1984. V.75. N 1. P.173-185.

35. Arase T., Arase E.M. Deep-sea ambient noise statistics // J.Acoust.Soc.Am. 1968. V.44. N 12. P.1936-1952.

36. Arase E.M., Arase T. Ambient sea noise in the deep and shallow ocean// Acoust.Soc.Am. 1967. V.42. N 1. P.73-77.

37. Mc Connell S.O., Schilt M.P., Dworski J.G. Ambient noise measurements from 100 Hz to 80 kHz in an Alaskan fjord// Acoust.Soc.Am. 1992. V.91. N 4. P.1998-2003.

38. Ingenito F., Wolf S.N. Site dependence of wind-dominated ambient noise in shallow water.// Acoust.Soc.Am. 1989. V.85. N 1. P.141-145.

39. Ewing W.M., Jardetzky W.S., Press F. Elastic waves in layered media. New York. McGraw-Hill. 1957.

40. DeSanto J.A. Theoretical methods in ocean acoustics. In: Ocean acoustics. / Ed J.A.DeSanto. New York . Springer-Verlag 1979.

41. DiNapoli F.R., Deavenport R.L. Numerical models of underwater acoustic propagation. In: Ocean acoustics. / Ed J.A.DeSanto. New York . Springer- Verlag 1979.

42. Maltsev N.E. Mathematical modelling of sound fields in ocean. In : Ocean acoustics : Modern state. /Ed. L.M.Brekhovskikh, I.B.Andreeva. Moscow. Nauka. 1982. (in Russian).

43. Tappert F.D. The parabolic approximation method. In : Wave propagation and underwater acoustics./Ed.J.B.Keller J.S.Papadakis. New York. Springer-Verlag. 1977.

44. Vefring E.H.,S.Mjolsnes. A parabolic wave equation based on rational-cubic approximation. // J.Acoust.Soc.Am. 1990. V.87. P.619-623.

45. McDaniel S.T. Propagation of normal mode in the parabolic approximation. //J.Acoust.Soc.Amer. 1975. V.57 P.307-311.

46. St.Mary D.F., Lee D., Botseas G A modified wide angle parabolic wave equation // J.Comput.Phys. 1987. V.71. P. 304-315.

47. Claerbout J.F. Fundamentals of geophysical data processing New York. McGraw-Hill. 1976.

48. Greene R.R. The rational approximation to the acoustic wave equation with bottom interaction.//J.Acoust.Soc.Am. 1984. V.76. P.1764-1773.

49. Knightly G.H.,Lee D.,St.Mary D.F. A high-order parabolic wave equation. //J.Acoust.Soc.Am. 1987. V.82. P.580-587.

50. Ahluwalia D.S., Keller J.B. Exact and asymptotic representations of sound field in stratified ocean. In : Wave propagation and underwater acoustics./Ed.J.B.Keller J.S.Papadakis. New York. Springer-Verlag. 1977.

51. Belov A.I. Calculation of sound field in shallow water using cross-section method in adiabatic approach.// Proc. of the II conference on numerical methods in modern acoustic problems. Moscow. 1988. (in Russian).

52. Belov A.I., Lebedev O.V. Calculation of sound field in shallow water using parabolic equation method.// Proc. of the II conference on numerical methods in modern acoustic problems. Moskow. 1988. (in Russian).